2008

Tuning of the Active Hair Bundle

Omar Ahmad

Tuning of the Active Hair Bundle

A Thesis Presented to the Faculty of
The Rockefeller University
In Partial Fulfillment of the Requirements for
the Degree of Doctor of Philosophy

by
Omar Ahmad
June 2008

Tuning of the Active Hair Bundle

Omar Ahmad, Ph.D.
The Rockefeller University 2008

The organs of the inner ear rely upon a population of several thousand sensory *hair cells* to amplify and transduce acoustic, seismic, and kinesthetic signals. Each hair cell detects mechanical disturbances by means of its *hair bundle*, a motile organelle consisting of actin-filled, villous projections (called *stereocilia*) endowed with assemblies (called *adaptation motors*) of mechano-sensitive ion channels and myosin molecules that power both spontaneous and evoked movements. Active hair-bundle motility serves two functions: it mechanically amplifies sensory stimuli; and it regulates their transduction into electrical signals that drive the hair-cell synapse. To characterize these two functions, we consider here a model of the mechanical and electrical dynamics of the hair bundle of the bullfrog sacculus. Under simplifying assumptions, we reduce this model to a two-dimensional dynamical system resembling the Hill model of a muscle fiber, and outline a procedure for estimating its parameters from experiment. We delineate the bifurcation structure of this simplified model, and analyse by perturbation methods its behavior in various dynamical regimes, notably in the relaxation-oscillation regime that displays prominently the hair bundle's active process; and in the near-Hopf-bifurcation regime at which auditory hair cells are thought to operate *in vivo*. We find close similarities between the dynamics of the active hair bundle and those of simplified models of a spiking neuron. In light of this analysis, we offer an account of the biophysical mechanisms underlying

the spontaneous oscillations, frequency specificity, nonlinear gain, and self-tuning predicted for auditory hair bundles poised near a Hopf bifurcation.

Acknowledgements

First and foremost, I would like to thank my teachers: Jim Hudspeth and Bruce Knight who have guided my study of neuroscience; Mario Bunge, Mike Mackey, and Jeff Wiseman who instilled in me an appreciation for science, and encouraged me to pursue research; and Victor Garaway who taught me how to write. I would also like to thank Albert Libchaber, Marcelo Magnasco, Mike Shelley, and Sid Strickland for their helpful comments and advice.

I am grateful to Mark Andermann, Daniel Andor, Tim Austin, Alok Bhardwaj, Dolores Bozovic, Samidh Chakrabarti, Brian Fabella, Paul Francois, Jacob Goldfield, David Jordan, Jeff Kim, Sagar Koduri, Ramesh Kathanadhi, Lukasz Kowalik, Adria Leboeuf, Julie Ann Miller, Maria Neimark, Tanya Nguyen, Tarje Nissen-Meyer, Dan Reuman, Thomas Risler, Jan Skotheim, and Matt Wright for their many insightful intellectual contributions to this work.

Finally, I would like to dedicate this thesis to my family, whose constant

support and encouragement have inspired me in all aspects of my life.

Contents

List of Figures

List of Tables

Chapter 1

Introduction

Animal nervous systems use both static tuning and feedback to regulate the allocation of scarce physiological resources to mechanisms for sensing, processing, and responding to natural stimuli. A hunting bat, for instance, adjusts through cortical feedback both the electro-mechanical tuning of its auditory organ [22] and the emission pattern of its echolocating cries to match the physical features of its acoustic environment and its prey [18]. The mantid that it hunts, with its single cyclopean ear tuned to the ultrasound range of the bat's vocalizations [20], discerns by audition the stalking tactics of its pursuer as it times its escape.

Hair cells of the vertebrate inner ear transduce mechanical signals that vary greatly in their frequency, intensity, and duration. The microbat cochlea, for instance, detects sounds as high as 100 kHz [16], with a hearing threshold of -20 dB at mid-range frequencies. At the opposite end of the frequency range, the sacculus of the white-lipped toad responds to seismic

accelerations as faint as $10^{-6} m.s^{-2}$ [15].

Despite the breadth of signals detected by the inner ear, data on the development, morphology, physiology, and molecular constitution of the hair bundle point to a core, conserved set of mechanisms operating in this organelle throughout the organs of the inner ear and across vertebrate species. This suggests that the same core mechanisms of the hair bundle are appropriately tuned in each organ of the inner ear to suit the signals for which that organ is specialized. For instance, cochlear hair bundles may self-tune to near an oscillatory instability called a *Hopf bifurcation* [7, 3], a setting that would confer the frequency specificity, non-linear gain, and propensity for spontaneous activity manifested by this organ.

Below, we consider three questions: 1) How do the mechanical, electrical, and biochemical properties of the hair bundle give rise to the nonlinear oscillations it exhibits *in vitro*? 2) How do these properties shape the nonlinear response of the hair bundle to mechanical stimulation? 3) Which of these properties might the hair cell regulate *in vivo* to adjust the proximity of its hair bundle's dynamics to a Hopf bifurcation?

To address these questions, we elaborate a biophysically detailed model of the hair bundle of the bullfrog sacculus, a system that has been extensively characterized both experimentally and theoretically. The detailed model incorporates assumptions about the mechanics of the stereocilia; the kinetics of the transduction channels; the mechanics of the adaptation motors; and

the electrophysiology of the hair cell.

Under plausible simplifying assumptions, the detailed model reduces to a dynamical system with two degrees of freedom, which we call the *simplified model*. We consider two mechanistic forms of the simplified model that represent, variously, the hair bundle's internal dynamics and its input-output structure. From this pair of mechanistic forms, we derive a phenomenological form of the simplified model that resembles the van der Pol-Duffing equation, and that corresponds to an analysis of the hair bundle into a passive, linear second-order system coupled through feedback to an active nonlinear amplifying element.

This phenomenological description yields a biophysical interpretation for the conditions of a Hopf bifurcation; at a Hopf bifurcation, the active mechanism of the hair bundle ensures both that the contractile force triggered by a weak mechanical disturbance exactly counterbalances the effective viscous force acting upon the bundle; and that the effective elastic force upon the bundle is restorative, despite the observed negative stiffness of the nonlinear elastic elements that gate the bundle's transduction channels.

In addition, the phenomenological form of the model allows us to explain, in terms of the interplay of effective viscous, elastic, and inertial forces, the biophysical mechanisms that give rise to the spontaneous oscillations, frequency specificity, nonlinear gain, and self-tuning hypothesized to occur in auditory hair bundles.

In section 2 below, we describe in outline a detailed model of the hair bundle, and explain its reduction to the simplified model that we subsequently analyse. In section 3, we characterize the bifurcation structure of the simplified model, and demonstrate its ressemblance to that of the Fitzhugh-Nagumo model of a spiking neuron. In section 4, we apply asymptotic and numerical methods to characterize the self-induced, nonlinear oscillations of the active hair bundle observed *in vitro*. In section 5, we study the response of the stable, active bundle to sinusoidal mechanical forcing. In section 6, we examine the hypothesis that the auditory hair cell tunes its bundle to a supercritical Hopf bifurcation by regulating the drag coefficient of the bundle's adaptation motor. In section 7, we discuss our results.

Chapter 2

A model of the active hair bundle

2.1 Detailed model and its simplification

The detailed model that we analyse comprises seven coupled ordinary differential equations describing four aspects of the hair bundle, namely: i) the mechanics of the stereocilia; ii) the kinetics of the mechanosensitive transduction channels; iii) the mechanics of the adaptation motor; and iv) the electro-physiology of the hair cell. In section (1) of the supplementary material, we discuss at length the variables, parameters, and dynamical equations of the detailed model, and the procedure by which we simplify it. Here, we enumerate the detailed model's key assumptions, and the additional assumptions required to obtain the simplified form that we analyse.

2.1.1 Assumptions of the detailed model

Stereociliary mechanics: The stereocilia behave as cantilevered beams immersed in a viscous fluid. The beams pivot about their bases and are mechanically coupled to one another in parallel [11] . The compliance of the hair bundle is a nonlinear function of the extension of elastic elements, called the *gating springs* [8], that stretch upon deflection of the bundle, and that set the transduction channels' propensity to conduct cation.

Transduction-channel kinetics: Each transduction channel possesses two states, an *open* state in which it conducts cation, and a *closed* state in which it is impermeable. The transition rates between the open and closed states obey Arrhenius relations [5], for which the activation energies vary linearly with the stretch imposed upon the gating springs.

Mechanics of the adaptation motor: The *adaptation motor* consists of an assembly of myosin molecules that climb and slip along the actin cores of the stereocilia. The affinity of the adaptation motor for actin decreases with increasing intracellular Ca^{2+} concentration. The adaptation motor affects the mechanics of the stereocilia through the stretch that it imposes upon the gating spring. Its movement within the bundle is constrained both by an extent spring and a non-linear limiting element [17].

Electrophysiology of the hair cell: The electrical response of the cell provides feedback by adjusting the Ca^{2+} concentration in the vicinity of the adaptation motor. The Ca^{2+} current is determined by an electrochemical gradient driving the entry of Ca^{2+} into the hair cell, and satisfies the Goldman-Hodgkin-Katz equation [14]. The flow of K^{+} ion affects the driving force for the entry of Ca^{2+} through its influence upon the membrane potential [2].

2.1.2 Simplification of the detailed model

The detailed model is challenging to investigate both because of technical limitations in measuring experimentally the many biophysical quantities that enter into it; and because of the mathematical complexity of analysing a dynamical system involving many parameters and variables. For these reasons, we seek to approximate it with a simplified model whose parameters may be measured directly from *in vitro* experiments, and whose mathematical structure is amenable to phase-plane methods and to perturbation analysis.

To reduce the detailed model, we introduce six simplifying assumptions:

1. The system operates at low Reynolds number;

2. The dynamics of four rapidly-evolving variables of the detailed model (related to the dynamics of the channels and motors) may on slow time-scales be regarded as effectively always at steady-state;

3. The reverse electro-mechanical coupling between the voltage and the force of the adaptation motor is negligible;

4. The motor drag depends only weakly on the Ca^{2+} concentration;

5. The fraction p_b of motors bound to the actin core of the hair bundle varies linearly with the local Ca^{2+} concentration in the vicinity of the adaptation motor.

6. The nonlinearity in the motor force that limits adaptation associated with negative displacements ofthe bundle is absent within the range of bundle motion considered.

Under assumption (1), we neglect the mass of the hair bundle. Under assumption (2), we replace the dynamical equations for the rapidly-evolving variables with algebraic or transcendental equations that describe their de-

pendence at steady state upon the remaining slow variables. Under assumption (3), we neglect the dynamical equation for the voltage when considering the hair bundle's mechanical response. Assumptions (4)-(6) simplify the form of the nonlinearity in the dynamical equation for the adaptation motor.

2.1.3 Mechanistic forms of the simplified model

Extension-resetting form of the simplified model

The preceding six assumptions reduce the detailed model to a simplified model, illustrated in Figure 2.1. This simplified model consists of two dimensionless ordinary differential equations that govern a fast activating variable χ representing the (scaled) extension of the gating spring, and a slow resetting variable X_a representing the (scaled) position of the adaptation motor:

$$\frac{d}{dt}\begin{pmatrix} \chi \\ X_a \end{pmatrix} = \begin{pmatrix} \Phi_{FN,\chi} \\ \Phi_{FN,X_a} \end{pmatrix} = \begin{pmatrix} (\kappa - \varepsilon\kappa_a)(\Psi_\chi - X_a) \\ \varepsilon\kappa_a(\Psi_a - X_a) \end{pmatrix} \tag{2.1}$$

Ψ_χ and Ψ_a are the χ- and X_a-*nullcline functions*, along which the velocities of χ and X_a, respectively, vanish, and p_o is the (quasi) steady-state *open probability* of the transduction channels:

$$\Psi_\chi \equiv \Psi_\chi(\chi) =_{df} \frac{1}{\kappa - \varepsilon\kappa_a}\left(-(1+\varepsilon)\chi + (\eta - \varepsilon\eta_a)\, p_o(\chi) + C\right) \tag{2.2}$$

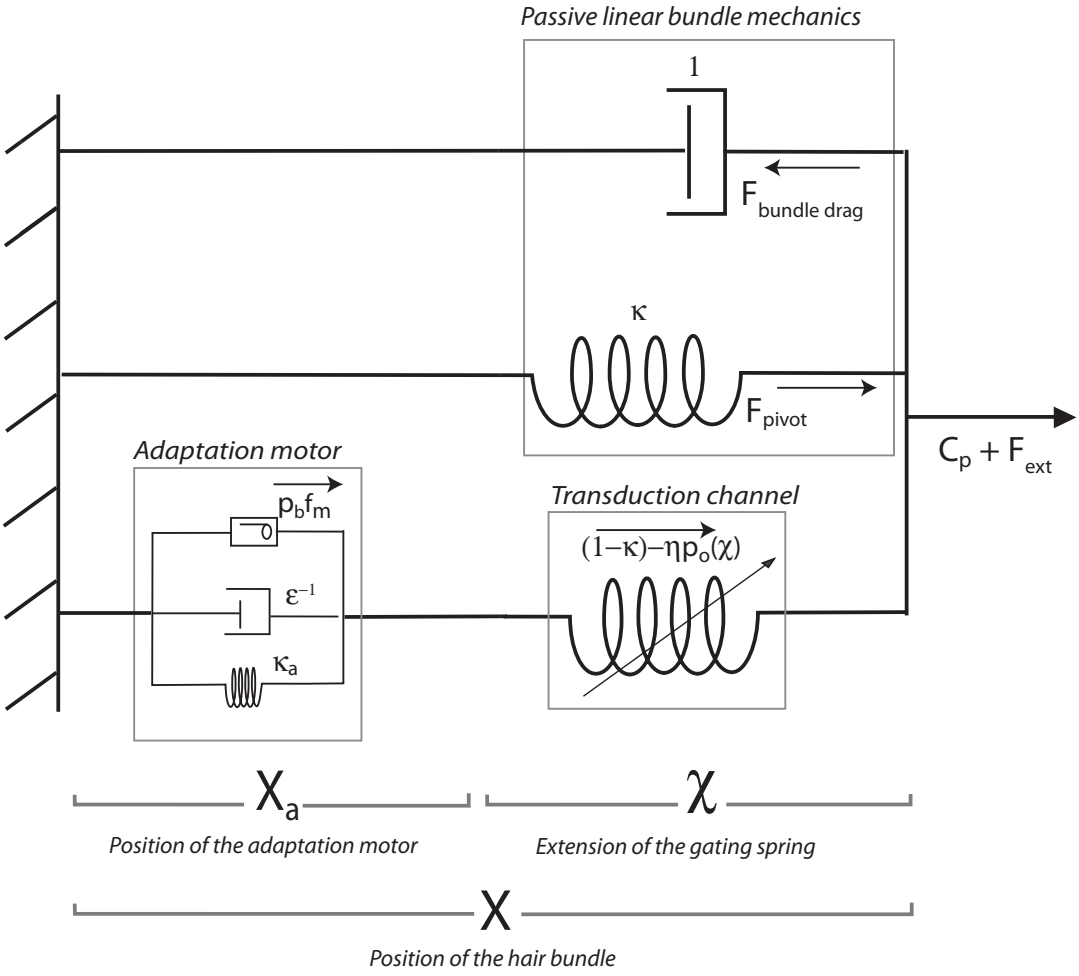

Figure 2.1: *Mechanistic description of the simplified model*
The diagram shows a nonlinear elastic element (labeled *transduction channel*) in series with a contractile element (labeled *adaptation motor*). The adaptation motor consists of a force-generating element (indicated by the "active walker" caricature of a myosin molecule) in parallel with a Hookean extent spring. In parallel with the adaptation motor and the transduction channels are the stereociliary pivots of the hair bundle, which have linear elastic properties. Energy dissipation occurs both through hydrodynamic drag upon the hair bundle (indicated by the dashpot in parallel with the pivots) and through internal dissipation by the adaptation motor, (labeled with a dashpot in parallel with the active walker). Symbols with arrows indicate forces; the remaining symbols denote parameters of the model.

$$\Psi_a \equiv \Psi_a(\chi) =_{df} \frac{1}{\kappa_a}(\chi + \eta_a p_o(\chi)) \tag{2.3}$$

$$p_o(\chi) =_{df} \frac{1}{1 + exp(-\chi)} \tag{2.4}$$

The six dimensionless parameters ε, η, η_a, κ, κ_a, and C that occur in (2.1)-(2.3) satisfy the constraints:

$$0 < \varepsilon \quad , \quad 0 < \kappa < 1 \quad , \quad 0 < \kappa_a \quad , \quad 0 < \eta \quad , \quad -\eta < \eta_a, \quad , \quad -\infty < C < \infty \tag{2.5}$$

We refer to equations (2.1)-(2.5) as the *extension-resetting* form (or (χ, X_a)–form) of the simplified model.

It follows from equation (2.1) that at fixed X_a, the velocity of χ is given by the negative gradient of the *elastic potential function* U:

$$\frac{d\chi}{dt} = -\frac{dU}{d\chi} \tag{2.6}$$

$$U(\chi, X_a) =_{df} -C\chi + (\kappa - \varepsilon\kappa_a)\chi X_a + (1+\varepsilon)\frac{\chi^2}{2} - (\eta - \varepsilon\eta_a)\left(ln\left(1 + e^{\chi}\right) - ln(2)\right) \tag{2.7}$$

where we have chosen by convention the constant term in (2.31) such that U vanishes at the point $(\chi, X_a) = (0, 0)$.

We can assign physical interpetations to the six parameters (ε, η, η_a, κ, κ_a, and C) of the simplified model:

ε : The *time-scale parameter* ε corresponds to the ratio of the time-scale of fast movement of the bundle to the time-scale for the slow movement of the adaptation motor. This ratio varies inversely with the drag coefficient of the adaptation motor.

η : The *gating nonlinearity parameter* η determines the influence upon χ of the non-linearity due to the gating compliance. η varies directly with the stiffness of the gating springs, and inversely with the temperature. $\eta > 4$ corresponds to the regime of negative hair-bundle stiffness.

η_a : The *motor nonlinearity parameter* η_a determines the influence upon X_a of the non-linearities arising from the gating compliance and from the Ca^{2+} sensitivity of the adaptation motor. It varies directly both

with the sensitivity of the motors to Ca^{2+} and with the maximal climbing force of the adaptation motors. The condition $\eta_a = 0$ corresponds to the regime in which the slipping force due to a Ca^{2+}-induced change in the fraction of motor associated with actin exactly counterbalances the change in elastic force due to length changes of the nonlinear gating spring. $\eta_a = -\eta$ corresponds to the motors being either inactive or insensitive to Ca^{2+}. The sum $\eta + \eta_a$ is the maximal force that can exerted by the adaptation motor.

κ : The *pivot stiffness coefficient* κ determines the influence upon the gating extension χ of the motor position X_a; κ corresponds to the fraction of the total stiffness of the bundle contributed by the stereociliary pivots.

κ_a : The *extent-spring stiffness coefficient* κ_a describes elastic elements internal to the bundle that constrain the movement of the adaptation motor.

C : The *scaled static force* C is proportional to the difference between the static force on the stereociliary pivots and the maximal climbing force of the adaptation motor.

The nullcline functions Ψ_χ and Ψ_a may be inferred from the force-

displacement and current-displacement functions measured under displacement clamp:

$$\Psi_\chi\left(X_{clamped} + X^*_{a,ref}\right) = \frac{1}{(\kappa - \varepsilon\kappa_a)} F_0\left(X_{clamped}\right) \tag{2.8}$$

$$\Psi_a\left(X_{clamped} + X^*_{a,ref}\right) = \frac{1}{\kappa_a}\left(X_{clamped} - Log\left(\frac{I_{HB}/I_{\max}}{1 - I_{HB}/I_{\max}}\right)\right) \tag{2.9}$$

where F_0 represents the scaled instantaneous force-displacement function measured under displacement clamp; $X_{clamped}$ denotes the scaled displacement imposed upon the bundle by the displacement clamp; and X^*_a denotes the scaled steady-state position of the adaptation motor at rest. The shape of the nullclines can be shown to yield estimates of the five *structural* parameters η, η_a, κ, κ_a, and C. The remaining time-scale parameter ε can be measured by fitting the temporal trajectories of the force or current measured under displacement clamp.

Section (2) of the supplementary material discusses in greater depth the problem of parameter estimation.

Force-displacement form of the simplified model

An alternative formulation of the simplified model takes as variables the

fractional active force ϕ of the adaptation motor; and the scaled displacement X of the hair bundle:

$$\phi =_{df} 1 - p_o = \frac{\exp[-\chi]}{1 + \exp[-\chi]} \tag{2.10}$$

$$X =_{df} \chi + X_a \tag{2.11}$$

The change of variables specified by equation (2.10), applied to the dynamical equation (2.1), yields the *force-displacement* form, or ((ϕ, X)– form) of the simplified model:

$$\frac{d}{dt}\begin{pmatrix} \phi \\ X \end{pmatrix} = \begin{pmatrix} \Phi_{Hill,\phi} \\ \Phi_{Hill,X} \end{pmatrix} = \begin{pmatrix} -(\kappa - \varepsilon\kappa_a)\,\phi\,(1-\phi)\,(H_\phi - X) \\ \kappa\,(H_X - X) \end{pmatrix} \tag{2.12}$$

where H_ϕ is the *ϕ-nullcline function*, along which the rate of change of the active force vanishes, and H_X is the *X-nullcline function*, along which the velocity of X vanishes:

$$H_\phi(\phi) =_{df} \frac{1}{\kappa - \varepsilon\kappa_a}\left[C + (\eta - \varepsilon\eta_a) + (1 + \varepsilon(1 + \kappa_a) - \kappa)\ln\left[\frac{\phi}{1-\phi}\right] - (\eta - \varepsilon\eta_a)\phi\right] \tag{2.13}$$

$$H_X(\phi) =_{df} \frac{1}{\kappa}\left[(C + \eta) + (1 - \kappa)\ln\left[\frac{\phi}{1-\phi}\right] - \eta\phi\right] \tag{2.14}$$

To arrive at the force-displacement form, consider the relation between the open probability p_o and the activity of the adaptation motor. The motor is at its most active when $p_o = 0$ (i.e.: the transduction channels are completely shut), and the Ca^{2+} concentration in the stereocilia drops into the nanomolar range; the motor falls to its minimal level of activity when $p_o = 1$ (i.e.: the channels are completely open), and the stereocilia are flooded with Ca^{2+}. In general, the active process contributes a force term ϕ_u proportional to the fraction $p_b = 1 - Sp_o$ of myosin motors bound to the actin cores of the stereocilia:

$$\phi_u = (1 - Sp_o)f_m \tag{2.15}$$

where we have introduced the parameters f_m, S, and C_p to represent, respectively, the motor force, the motor sensitivity to Ca^{2+} and the passive static force:

$$\eta_a = Sf_m - \eta \qquad C = \frac{\kappa}{\kappa_a} f_m + C_p \tag{2.16}$$

We normalize the active force ϕ_u to define the *fractional active force* ϕ:

$$\phi =_{df} \frac{\phi_u - \phi_{u,min}}{\phi_{u,max} - \phi_{u,min}} = 1 - p_o \tag{2.17}$$

$$\phi_{u,min} = df \lim_{\chi \to -\infty} \phi_u = (1 - S) f_m \quad , \quad \lim_{\chi \to \infty} \phi_{u,max} = Sf_m \tag{2.18}$$

The force ϕ_u exerted by the motor at a given value of p_o is thus the maximal active force $(\eta + \eta_a)$ times the fractional active force $\phi = 1 - p_o$:

$$\phi_u = (\eta + \eta_a)(1 - p_o) = (\eta + \eta_a)\phi \tag{2.19}$$

2.1.4 Phenomenological forms of the simplified model

For each of the two mechanistic forms of the model presented above, we can construct an equivalent *phenomenological* form involving a single variable and its rate of change. Our approach will be to define effective viscous and elastic coefficients corresponding to the decay and oscillation time-scales arising in the linearized dynamics of the corresponding mechanistic form. The phenomenological forms of the model make possible a simple description of the system's energetics and feedback structure.

The extension-resetting form of the simplified model, comprising equations (2.1) - (2.5), is equivalent to a system (viz. (A.66) - (2.23) below) governed by a single, second-order nonlinear differential equation in χ:

$$\frac{d^2\chi}{dt^2} + \mu(\chi)\frac{d\chi}{dt} + \omega_\kappa^2\chi - \omega_\kappa^2 d_\kappa p_o(\chi) - \varepsilon\kappa_a C = 0 \tag{2.20}$$

where the *effective drag coefficient* $\mu(\chi)$ in the differential equation above is given by:

$$\mu(\chi) =_{df} (1 + \varepsilon + \varepsilon\kappa_a) - \alpha_\varepsilon p_o(\chi)\,(1 - p_o(\chi)) \tag{2.21}$$

The parameters α_ε, ω_κ, and d_κ introduced above are related to the parameters of the extension-resetting form by the equations:

$$\alpha_\varepsilon = \eta - \varepsilon\eta_a \quad , \quad \omega_\kappa = \sqrt{\varepsilon\,(\kappa + \kappa_a)} \quad , \quad d_\kappa = \frac{\kappa\kappa_a}{\kappa + \kappa_a}\left(\frac{\eta}{\kappa} - \frac{\eta_a}{\kappa_a}\right) \tag{2.22}$$

The six dimensionless parameters (α_ε, ε, κ_a, ω_κ, C, and d_κ) occurring in (A.66) - (A.67) satisfy the constraints:

$$-\frac{\omega_\kappa^2 d_\kappa}{\varepsilon\kappa_a} < \alpha_\varepsilon < d_\kappa(1+\varepsilon) \quad , \quad 0 < \varepsilon \quad , \quad 0 < \kappa_a \quad , \quad \sqrt{\varepsilon\kappa_a} < \omega_\kappa < \sqrt{\varepsilon(1+\kappa_a)} \tag{2.23}$$

We refer to equations (A.66) - (2.23) as the *phenomenological form in* χ of the simplified model.

To depict the dynamics of the simplified model on the $(\chi, \frac{d\chi}{dt})$ phase plane, we resolve the second-order equation (A.66) into a pair of first-order equations involving the variable χ and its velocity v:

$$\frac{d}{dt}\begin{pmatrix} \chi \\ v \end{pmatrix} = \begin{pmatrix} v \\ \mu(\chi)\left(\Psi_v(\chi) - v\right) \end{pmatrix} \tag{2.24}$$

The function Ψ_v corresponds to the *v-nullcline function*, the locus of points in the (χ, v) state space at which the acceleration of the gating extension χ vanishes.

$$\Psi_v(\chi) =_{df} \frac{-\omega_\kappa^2 \chi + \omega_\kappa^2 d_\kappa p_o(\chi) + \varepsilon \kappa_a C}{\mu(\chi)} \tag{2.25}$$

2.1.5 Force-balance and power-balance relations

The second-order differential equation (A.66) for the dynamics of χ, and hence the equivalent first-order equation (2.24), may be regarded as a force-balance equation for the gating elements. To make this explicit, we define effective inertial, viscous, and elastic forces:

$$F_{inertial} =_{df} \frac{dv}{dt} \quad , \quad F_{viscous} =_{df} -\mu(\chi)v \quad , \quad F_{elastic} =_{df} \mu(\chi)\Psi_v(\chi) \tag{2.26}$$

By equation (2.24), these forces obey the relation:

$$F_{inertial} = F_{viscous} + F_{elastic} \tag{2.27}$$

Although, at low Reynolds number, the hair bundle's mass negligible, its internal active force ϕ_u can act as a source of substantial acceleration; it is acceleration due to this force that gives rise to the term $F_{inertial}$. In light of this, we can interpret the v-nullcline function Φ_v as a *terminal velocity* function, in the sense that when $F_{inertial}$ is negligible, $F_{viscous}$ balances $F_{elastic}$, and $v = \Psi_v$. The defining equation (2.26) for $F_{viscous}$ corresponds to a constitutive relation between this force and the velocity v, in which μ occurs as a susceptibility.

$$\mu = -\frac{dF_{viscous}}{dv} \tag{2.28}$$

Integration of μ with respect to χ yields the *viscous force-velocity characteristic* $F_\mu(\chi)$ for the lumped resistive elements of the hair bundle:

$$F_\mu(\chi) =_{df} \int_{\chi^*}^{\chi} \mu(\chi')d\chi' = (1 + \varepsilon(1 + \kappa_a))\,(\chi - \chi^*) - \alpha_\varepsilon\,(p_o(\chi) - p_o(\chi^*)) \tag{2.29}$$

The function F_μ is the mechanical analog of the current-voltage characteristic describing the resistive elements of an electrical circuit.

Just as we defined an effective drag, so we can define the *effective stiffness* k_e as the susceptibility of the force $-F_{elastic}$ with respect to the variable χ:

$$k_e =_{df} -\frac{dF_{elastic}}{d\chi} \tag{2.30}$$

Integration of $F_{elastic}$ with respect to χ yields a potential-energy function describing the effective elastic energy as a function of the gating extension χ:

$$U_{elastic}(\chi) =_{df} -\varepsilon\kappa_a C\chi + \frac{1}{2}\omega_\kappa^2\chi^2 - \omega_\kappa^2 d_\kappa \left(ln\left(1+e^{\chi}\right) - ln(2)\right) \qquad (2.31)$$

where we have chosen the constant in the above equation such that $U_{elastic}(0) = 0$

In sum, the effective drag, stiffness, viscous force, elastic force, elastic potential, and viscous force-velocity characteristic are interrelated by virtue of their nonlinear dependence on χ:

$$k_e = \frac{d^2U_{elastic}}{d\chi^2} = -\frac{dF_{elastic}}{d\chi} = -\frac{d}{d\chi}\left[\mu\ \Psi_v\right] = -\frac{d}{d\chi}\left[\frac{dF_\mu}{d\chi}\Psi_v\right] = \frac{d}{d\chi}\left[\frac{dF_{viscous}}{dv}\Psi_v\right] \qquad (2.32)$$

Since v is related to the extension and resetting variables χ and X_a through the potential function U given by equation (2.31), we can express the effective forces entirely in terms of χ and X_a:

$$F_{inertial}(\chi, X_a) = -\frac{d}{dt}\left(\frac{\partial U}{\partial \chi}\right) \quad , \quad F_{viscous}(\chi, X_a) = \mu\frac{\partial U}{\partial \chi} \quad , \quad F_{elastic}(\chi) = \mu_(\chi)\Psi_v(\chi) \qquad (2.33)$$

Accordingly, the force-balance equation (2.27), expressed in terms of χ and X_a, takes the form:

$$\frac{d}{dt}\left[\frac{dU}{d\chi}\right] = \mu\left(\frac{dU}{d\chi} - \Psi_v\right) \tag{2.34}$$

Just as we defined phenomenological inertial, viscous, and elastic forces, so we can define corresponding phenomenological kinetic, viscous, and elastic power functions associated with the gating extension χ:

$$P_{kinetic}(v) = \frac{d}{dt}\left[\frac{1}{2}v^2\right] \quad , \quad P_{kinetic}(\chi, X_a) = \frac{d}{dt}\left[\frac{1}{2}\left(\frac{\partial U}{\partial \chi}\right)^2\right] \tag{2.35}$$

$$P_{viscous}(\chi, v) = F_{viscous}v \quad , \quad P_{viscous}(\chi, X_a) = -\mu(\chi)\left(\frac{\partial U}{\partial \chi}\right)^2 \tag{2.36}$$

$$P_{elastic}(\chi, v) = F_{elastic}v \quad , \quad P_{elastic}(\chi, X_a) = -F_{elastic}\frac{\partial U}{\partial \chi} \tag{2.37}$$

Like the phenomenological force functions, the power functions above satisfy a balance equation:

$$P_{kinetic} = P_{viscous} + P_{elastic} \tag{2.38}$$

The force-balance and power-balance relations derived above prove useful (as accounting devices) in later sections, where we carry out an asymptotic analysis of the hair bundle's spontaneous and stimulated dynamics. By virtue of the systematic relations (e.g.: equation (2.34)) between the mechanistic and phenomenological forms of the model, any description of the system's dynamics in terms the effective force and power functions above may readily be translated into a corresponding explanation in terms of the hair bundle's biophysical mechanisms.

2.2 Relations between the mechanistic and phenomenological forms

2.2.1 Extension-resetting form and the phenomenological form in χ

To clarify the relation between the mechanistic and phenomenological forms of the model, let us consider the linear operator A defined by the linearization of the dynamical system in equation (2.1):

$$A =_{df}= \begin{pmatrix} \frac{d}{d\chi}\Phi_{FN,\chi} & \frac{d}{dX_a}\Phi_{FN,\chi} \\ \frac{d}{d\chi}\Phi_{FN,X_a} & \frac{d}{dX_a}\Phi_{FN,X_a} \end{pmatrix} = \begin{pmatrix} (\kappa - \varepsilon\kappa_a)\frac{\partial\Psi_\chi}{\partial\chi} & \varepsilon\kappa_a - \kappa \\ \varepsilon\kappa_a\frac{\partial\Psi_a}{\partial\chi} & -\varepsilon\kappa_a \end{pmatrix} \tag{2.39}$$

The operator A has eigenvalues:

$$\lambda_\pm = \frac{1}{2}\left[Tr_A \pm \sqrt{Tr_A^2 - 4Det_A}\right] \tag{2.40}$$

where Tr_A and Det_A are, respectively, the trace and determinant of A:

$$\begin{aligned} Tr_A \equiv Tr_A(\chi) &= \kappa\frac{\partial\Psi_\chi}{\partial\chi} - \varepsilon\kappa_a(1 + \frac{\partial\Psi_\chi}{\partial\chi}) \\ &= 1 + \varepsilon(1+\kappa) - \alpha_\varepsilon p_o(1-p_o) \end{aligned} \tag{2.41}$$

$$
\begin{aligned}
Det_A \equiv Det_A(\chi) &= \varepsilon\kappa_a\kappa\left(\frac{\partial\Psi_a}{\partial\chi}-\frac{\partial\Psi_\chi}{\partial\chi}\right)-\varepsilon^2\kappa_a^2\left(\frac{\partial\Psi_a}{\partial\chi}-\frac{\partial\Psi_\chi}{\partial\chi}\right) \\
&= \omega_\kappa^2\left(1-d_\kappa p_o(\chi)(1-p_o(\chi))\right)
\end{aligned}
\tag{2.42}
$$

Thus, in terms of the functions Tr_A and Det_A, equation (A.66) assumes the form:

$$
\frac{d^2\chi}{dt^2}-Tr_A\frac{d\chi}{dt}+\int_0^\chi Det_A(\chi')\,d\chi'-\left(\varepsilon\kappa_a C+\frac{\omega_\kappa^2 d_\kappa}{2}\right)=0 \tag{2.43}
$$

It follows that the function $-Tr_A(\chi)$ corresponds to the effective drag function $\mu(\chi)$ associated with the motion of χ, while $Det_A(\chi)$ corresponds to the phenomenological stiffness:

$$
Tr_A=-\mu \quad , \quad Det_A=k_e \tag{2.44}
$$

Det_A and Tr_A are interrelated by the equation:

$$Det_A = -\varepsilon\kappa_a \left(Tr_A + \kappa \frac{\partial \Psi_a}{\partial \chi} \right) - (\varepsilon\kappa_a)^2 \left(1 + \frac{\partial \Psi_a}{\partial \chi} \right) \tag{2.45}$$

Or, more succinctly,

$$\frac{d}{d\chi} \left[Tr_A \Psi_v \right] = Det_A \tag{2.46}$$

The functions Det_A and Tr_A above help us to interpret the parameters α_ε, ω_κ^2, and d_κ. We observe that

$$\alpha_\varepsilon = 4\left(\mu_\infty - \mu_0\right) \quad , \quad \omega_\kappa^2 = k_\infty \quad , \quad d_\kappa = 4\left(\frac{k_\infty - k_0}{k_\infty} \right) \tag{2.47}$$

where

$$k_0 =_{df} Det_A(0) \quad , \quad k_\infty =_{df} \lim_{|\chi| \to \infty} Det_A(\chi) \tag{2.48}$$

$$\mu_0 =_{df} -Tr_A(0) \quad , \quad \mu_\infty =_{df} -\lim_{|\chi|\to\infty} Tr_A(\chi) \tag{2.49}$$

Thus, α_ε is linear in the maximal increment of the phenomenological drag coefficient; ω_κ^2 represents the asymptotic phenomenological stiffness Det_A; and d_κ is proportional to the maximal relative increment in the phenomenological stiffness Det_A.

2.2.2 Force-displacement form and the phenomenological form in ϕ

Similar relations obtain between the force-displacement model and a phenomenological model in the variable ϕ. Let B denote the linearized evolution operator for the equations (2.13)-(2.14)

$$B =_{df} \begin{pmatrix} \frac{d}{dX}\Phi_{Hill,X} & \frac{d}{d\phi}\Phi_{Hill,X} \\ \frac{d}{dX}\Phi_{Hill,\phi} & \frac{d}{d\phi}\Phi_{Hill,\phi} \end{pmatrix} = \begin{pmatrix} (\kappa - \varepsilon\kappa_a)\frac{d}{d\phi}H_\phi & -(\kappa - \varepsilon\kappa_a) \\ \kappa\frac{d}{d\varphi}H_\phi & -\kappa \end{pmatrix} \tag{2.50}$$

Let Tr_B and Det_B denote, respectively, the trace and determinant of B. Just as we did above for the gating extension χ, we can give a phenomenological description of the models dynamics in terms of the active force ϕ and its rate of change ζ.

$$\frac{d}{dt}\begin{pmatrix} \phi \\ \zeta \end{pmatrix} = \begin{pmatrix} \zeta \\ Tr_B\left(\zeta - \Psi_\zeta(\chi)\right) \end{pmatrix} \tag{2.51}$$

$$\frac{d\zeta}{dt} = Tr_B\left(\zeta - H_\zeta(\phi)\right) \tag{2.52}$$

where H_ζ is the $\zeta-$ nullcline function. Det_B and Tr_B are related to one another by:

$$\frac{d}{d\phi}\left[Tr_B H_\zeta\right] = Det_B \tag{2.53}$$

Integration of the state function for ϕ gives a potential function U_ϕ whose derivative is related to the rate of change of ϕ according to

$$\zeta = -\frac{dU_\phi}{d\phi} \tag{2.54}$$

2.3 Physical interpretation of the phenomenological form

The phenomenological form of the model allows us to regard the system as consisting of a passive linear sub-system involving χ coupled through feedback to an active non-linear sub-system involving the fractional active force ϕ. To demonstrate this, we cast the phenomenological equation in the form:

$$\frac{d^2\chi}{dt^2} + \mu_\infty \frac{d\chi}{dt} + k_\infty \chi = F_{Ph,active}\left(\phi, \zeta\right) \tag{2.55}$$

$$F_{Ph,active}\left(\phi, \zeta\right) =_{df} -\mu_f \zeta - k_f \phi + C_f \tag{2.56}$$

where the effective passive parameters μ_∞ and k_∞ are defined by:

$$\mu_\infty = \lim_{\chi \to \infty} \mu(\chi) = 1 + \varepsilon(1 + \kappa_a) \quad , \quad k_\infty = \lim_{\chi \to \infty} k(\chi) = \omega_\kappa^2 \tag{2.57}$$

and the effective active parameters μ_f , k_f , and C_f are defined by:

$$\mu_f =_{df} \frac{d\mu}{d\zeta} = \alpha_\varepsilon \quad , \quad k_f =_{df} \frac{d\kappa}{d\phi} = \omega_\kappa^2 d_\kappa \quad , \quad C_f = \varepsilon \kappa_a C \tag{2.58}$$

A schematic of the phenomenological form of the model is shown in Figure 2.2.

The analysis of the simplified model into a linear passive subsystem coupled through feedback to a nonlinear active subsystem brings into relief the hair bundle's similarity to both the van der Pol nonlinear electrical oscillator and the Duffing mechanical oscillator. In van der Pol's design, a linear RLC circuit is inductively coupled to an active nonlinear element (such as a vacuum tube or tunnel diode) that introduces an effective negative resistance for weak currents. In Duffing's apparatus, a horizontal metal rod with linear elastic properties clamped at both ends is coupled to an electromagnet that introduces an effective nonlinear stiffness for weak displacements. The hair-bundle model, as formulated in equation (2.55) can be seen to consist of an effective passive linear subsystem coupled to an active mechanism that introduces both effective nonlinear drag (through the term $\mu_f \zeta$) and effective nonlinear stiffness (through the term $k_f \phi$).

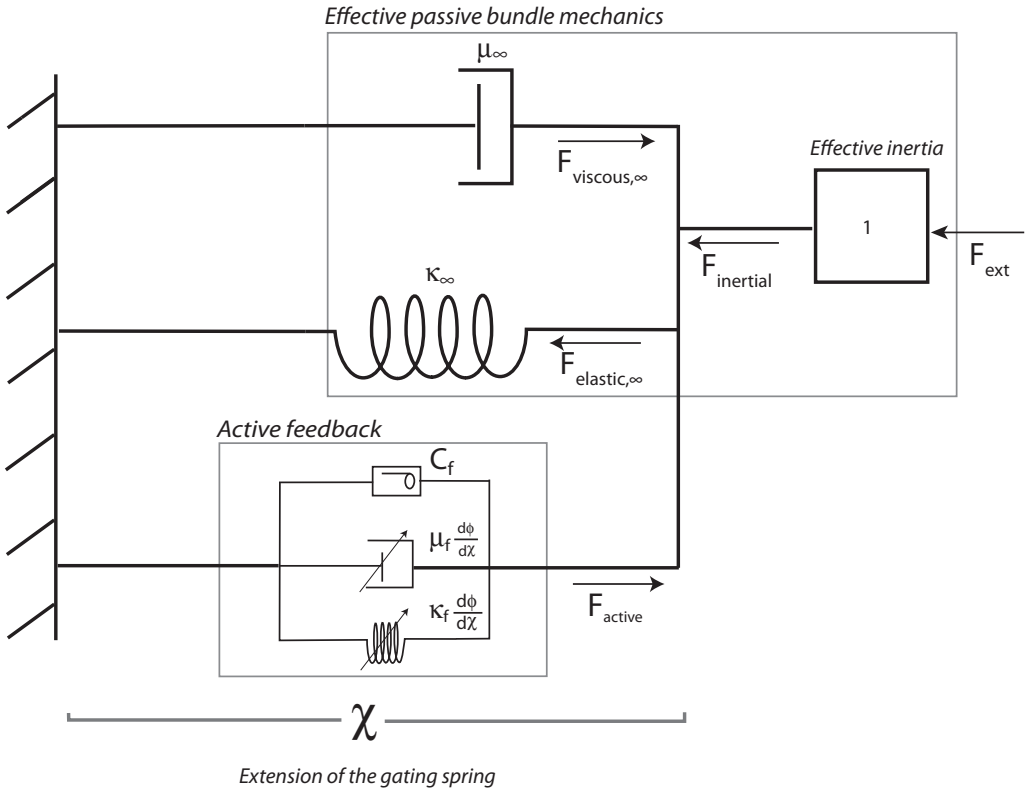

Figure 2.2: *Phenomenological form of the simplified model*
The phenomenological form of the simplified model can be seen to consist of a linear passive system (labeled *effective passive bundle mechanics*) coupled thorugh feedback to an active nonlinear mechanism (labeled *acitve feedback*)

These analogies to the van der Pol and Duffing oscillators motivate a physical interpretation for the six parameters α_ε, ε, κ_a, ω_κ, C, and d_κ of the phenomenological form of the model.

Three of these parameters– namely, the time-scale parameter ε, the extent-spring coupling coefficient κ_a, and the static force parameter C– are interpreted as in the case of the mechanistic forms. Regarding these parameters, we see that ε and κ_a together set the effective passive drag μ_∞, while the product $\varepsilon\kappa_a C$ constitutes the offset force C_f of the effective active system.

Below, we consider the remaining three parameters: α_ε, ω_κ, and d_κ:

α_ε : The *slipping parameter* (or *viscous coupling parameter*) α_ε consists of a weighted difference between the gating nonlinearity parameter η and motor nonlinearity parameter η_a, and is the coefficient μ_f of the effective active term $\frac{d\phi}{dt}$. It sets the slipping condition at which the effective viscosity vanishes (i.e.: $\mu = 0$), which at fixed χ^* occurs at the critical value $\alpha_{\varepsilon,slipping}$:

$$\alpha_{\varepsilon,slipping} \equiv \alpha_{\varepsilon,slipping}(\chi^*) = -\mu_\infty \left(\frac{d\phi}{d\chi}\right)^{-1}_{\chi=\chi^*} \tag{2.59}$$

For $\alpha_\varepsilon > \alpha_{\varepsilon,slipping}$, the effective viscosity at the operating point χ^* becomes negative, and hence χ^* becomes unstable.

ω_κ : The *natural frequency parameter* ω_κ varies as the square-root of both the time-scale parameter ε and the sum of the coupling parameters $\kappa_a + \kappa$, and its square corresponds to the stiffness k_∞ of the effective passive subsystem.

d_κ : The *buckling parameter* (or *elastic coupling parameter*) d_κ, also a weighted difference between the gating and motor nonlinearity parameters, occurs as the coefficient k_f of the force variable ϕ, rescaled by ω_κ^2. It sets the condition at which the effective stiffness k_e vanishes.

$$d_{\kappa,buckling} \equiv d_{\kappa,buckling}(\chi^*) = -\left(\frac{d\phi}{d\chi}\right)^{-1}_{\chi=\chi^*} \tag{2.60}$$

Thus, both the slipping parameter α_ε and the buckling parameter d_κ describe the balance between the gating nonlinearity η and the motor nonlinearity η_a, and correspond to couplling coefficients determining the interaction between the effective active and passive subsystems that compose the simplified model. From equations (2.59) - (2.60), the critical slipping and buckling parameters (at a fixed operating point χ^*) are related by:

$$\alpha_{\varepsilon,slipping} = \mu_\infty d_{\kappa,buckling} \tag{2.61}$$

2.3.1 Pade approximation of the simplified model

To further simplify the model, we use Pade approximation to replace the transcendental nullcline functions Ψ_χ and Ψ_a with rational functions.

The nullcline functions Ψ_χ and Ψ_a in the simplified model behave as linear functions in χ at large χ:

$$\Psi_\chi, \Psi_a \sim \chi \quad as \quad |\chi| \to \infty \tag{2.62}$$

In addition, Taylor expansion of Ψ_χ and Ψ_a about $\chi = 0$ gives, to cubic order:

$$\Psi_\chi(\chi) = \frac{1}{\kappa - \varepsilon\kappa_a}\left(-(1+\varepsilon)\,\chi + \frac{1}{48}\,(\eta - \varepsilon\eta_a)\,\chi^3 + O(\chi^4)\right) \tag{2.63}$$

$$\Psi_a(\chi) = \frac{1}{\kappa_a}\left(\chi + \frac{1}{48}\eta_a\chi^3 + O(\chi^4)\right) \tag{2.64}$$

These properties suggest approximating Ψ_χ and Ψ_a with rational functions that vary linearly with χ as $|\chi| \to \infty$ but exhibit a cubic nonlinearity near $\chi = 0$.

To obtain such functions, we construct the Pade approximants for Ψ_χ and Ψ_a of order $(3, 2)$ expanded about $\chi = 0$. The Pade approximant [1] of order (n, m) of a function f about $\chi = \chi_0$ is a rational function $R =_{df} \frac{P}{Q}$ (where P is a polynomial of degree n and Q is a polynomial of degree m) whose Taylor expansion about χ_0 agrees with the Taylor expansion of f about χ_0 up to order $n + m + 1$. We denote by N_χ and N_a the Pade approximants for Ψ_χ and Ψ_a, respectively.

Under the Pade approximation, the dynamical equations of the simplified model (i.e.: equation (2.1)) assume the form:

$$\frac{d\chi}{dt} = (\kappa - \varepsilon\kappa_a)\left(N_\chi(\chi) - X_a\right) \tag{2.65}$$

$$\frac{dX_a}{dt} = \varepsilon\kappa_a\left(N_a(\chi) - X_a\right) \tag{2.66}$$

where

$$N_\chi(\chi) = \frac{1}{\kappa - \varepsilon\kappa_a}\left[\left(\frac{\eta - \varepsilon\eta_a}{2} + C\right) - \left((1+\varepsilon) - \frac{1}{24}(\eta - \varepsilon\eta_a)\left(1 + \frac{50}{10+\chi^2}\right)\right)\chi\right] \tag{2.67}$$

$$N_a(\chi) = \frac{1}{\kappa_a}\left(\frac{\eta_a}{2} + \left(1 + \frac{1}{24}\eta_a\left(1 + \frac{50}{10+\chi^2}\right)\right)\chi\right) \tag{2.68}$$

Within the physiological range for the bundle's variables and parameters, the Pade-approximated nullcline functions N_χ and N_a agree closely with the transcendental functions Ψ_χ and Ψ_a. The accuracy of the approximation derives from fact that the Pade approximation places poles at $\pm i\sqrt{10}$, while the poles of the nullcline functions are at integral multiples of $i\pi$. As we will see in section (3.1), within the range of parameters and variables over which the Pade approximation is useful –which appears to include the whole physiological range of the system– the problem of determining the fixed points, eigenvalues, conditions for bifurcation, and normal-form coefficients for the system reduces to the problem of solving cubic and quadratic equations.

Section (3) of the supplementary material shows plots illustrating the quality of the Pade approximation.

2.4 Summary

In sum, we have reduced a detailed mechanistic model of the active hair bundle to two simplified mechanistic forms variously ressembling the Hill model of a muscle fiber and the Fitzhugh-Nagumo model of a neuron.

The extension-resetting form describes the dynamics of the hair bundle in terms of the internal variables χ and X_a. The force-displacement form, on the other hand, corresponds to an *input-output* description of the system. Sensory stimulation disturbs the position X of the bundle; this, in turn, induces a change in the transduction current, a quantity that varies linearly with the open probability p_o, and hence also with ϕ. Thus, force-displacement form, can equally be regarded as a current-displacement input-output form of the model.

The phenomenological forms ressemble the van der Pol and Duffing oscillators. Like the van der Pol and Duffing systems, the phenomenological forms of the simplified model allow us to regard the hair bundle as comprising a passive linear subsystem coupled through feedback to an active nonlinear subsystem.

In the sequel, we make use of the phenomenological form of the model to standardize our explanation of the role of various biophysical mechanisms

at play in the hair bundle. In view of the systematic relations (e.g.: equation (2.34)) between the phenomenological descriptions and the mechanistic descriptions from which they derive, the problem of explaining the bundle's mechanisms reduces to that of cataloguing its phenomenology.

Chapter 3

Bifurcation structure of the simplified model

The simplified hair-bundle model has a bifurcation structure that closely ressembles that of the Fitzhugh-Nagumo model of a neuron. Like the latter, the hair-bundle model variously exhibits excitability, bistability, and spontaneous oscillations.

Both models consist of nonlinear ordinary differential equations describing two variables, a fast (activating) and a slow (resetting) variable. The activating variable in the Fitzhugh-Nagumo model represents the membrane potential of the neuron and the gating variable for Na^+-channel activation, while the resetting variable represents the gating variables for both the neuron's K^+ channels and the inactivating mechanisms of its Na^+ channels. In the simplified hair-bundle model, the gating extension χ is the activating

variable while the motor position X_a is the resetting variable.

Inherent to both models are three distinct dynamical regimes: excitability, bistability, and spontaneous oscillations. Within the physiological range of parameters, the hair-bundle model can have either one, two or three fixed points. In each of these cases, the system can have a either no limit cycles, a single stable limit cycle, or an unstable limit cycle enclosed by a stable limit cycle.

In the basin of attraction of a stable fixed point in either model, three kinds of transients can occur: i) over-damped movements, in which the perturbed system decays exponentially back to the fixed point. ii) underdamped oscillations, in which the perturbed system undergoes nearly harmonic oscillations of decaying amplitude as it returns to the fixed point. iii) excitable dynamics, in which a sufficiently strong perturbation of the bundle produces a large excursion of the system, with its return to the steady state occurring through a slow resetting mechanism powered by the active process.

In the single-fixed-point regime, the fixed point can either be globally stable, in which case the system is excitable; or the fixed point can be unstable, in which case the system oscillates spontaneously. In the single-fixed-point excitable regime, both the hair-bundle model and the FitzHugh-Nagumo model show: i) an absence of all-or-none spikes and of true thresholds; ii) anodal break excitation, which in the hair bundle corresponds to fast adaptation; iii) spike acommodation; and iv) excitation block.

In the three-fixed-point regime, the system can have zero, one or two stable fixed points. In the case in which none of the three fixed points is stable, the system has a single stable limit cycle. In the case of a single stable fixed point, the system can either be excitable, with a true threshold; or it can exhibit spontaneous oscillations in which a stable limit cycle is separated from the stable fixed point by an unstable limit cycle. Finally, the system in the three-fixed point regime can have zero stable fixed points and a stable limit cycle; or it can have a single stable fixed point, and be either excitable or oscillatory; or it can be bistable, in which one of the fixed points is a saddle node and the other two are stable.

In contrast to the one and three fixed-point cases, which are structurally stable, the two-fixed-point case always corresponds to the point of a saddle-node bifurcation in the model.

Figure 3.1 shows phase portraits of the various dynamical regimes the simplified model can occupy.

Section (5) of the supplementary material considers in depth the excitable regime whose subthreshold behavior is underdamped, This regime illustrates many of the key features of the active hair bundle's nonlinear dynamics.

Name	Color	Definition
χ-nullcline	Black	$X_a = N_\chi(\chi)$
X_a-nullcline	Red	$X_a = N_a(\chi)$
v-nullcline	Blue	$\frac{dv}{dt} = \frac{dN_\chi}{d\chi}\frac{d\chi}{dt} - \frac{dX_a}{dt} = 0$
v_a-nullcline	Green	$\frac{d}{dt}X_a = \frac{dN_a}{d\chi}\frac{d\chi}{dt}$
X-nullcline	Dashed black	$\frac{dX}{dt} = \frac{d\chi}{dt} + \frac{dX_a}{dt} = 0$
u-nullcline	Dashed blue	$\frac{d^2X}{dt^2} = \frac{d^2\chi}{dt^2} + \frac{d^2X_a}{dt^2} = 0$
Forward-time integral curve	Orange	Forward integration of eqn. (2.1)
Backward-time integral curve	Gray	Backward integration of eqn. (2.1)

Table 3.1: *Legend for phase portraits.*
For phase portraits on the (χ, v) plane, X_a is treated as a function of χ and v through the smooth correspondence: $X_a(\chi, v) = \Psi_\chi - (\kappa - \varepsilon\kappa_a)^{-1}v$

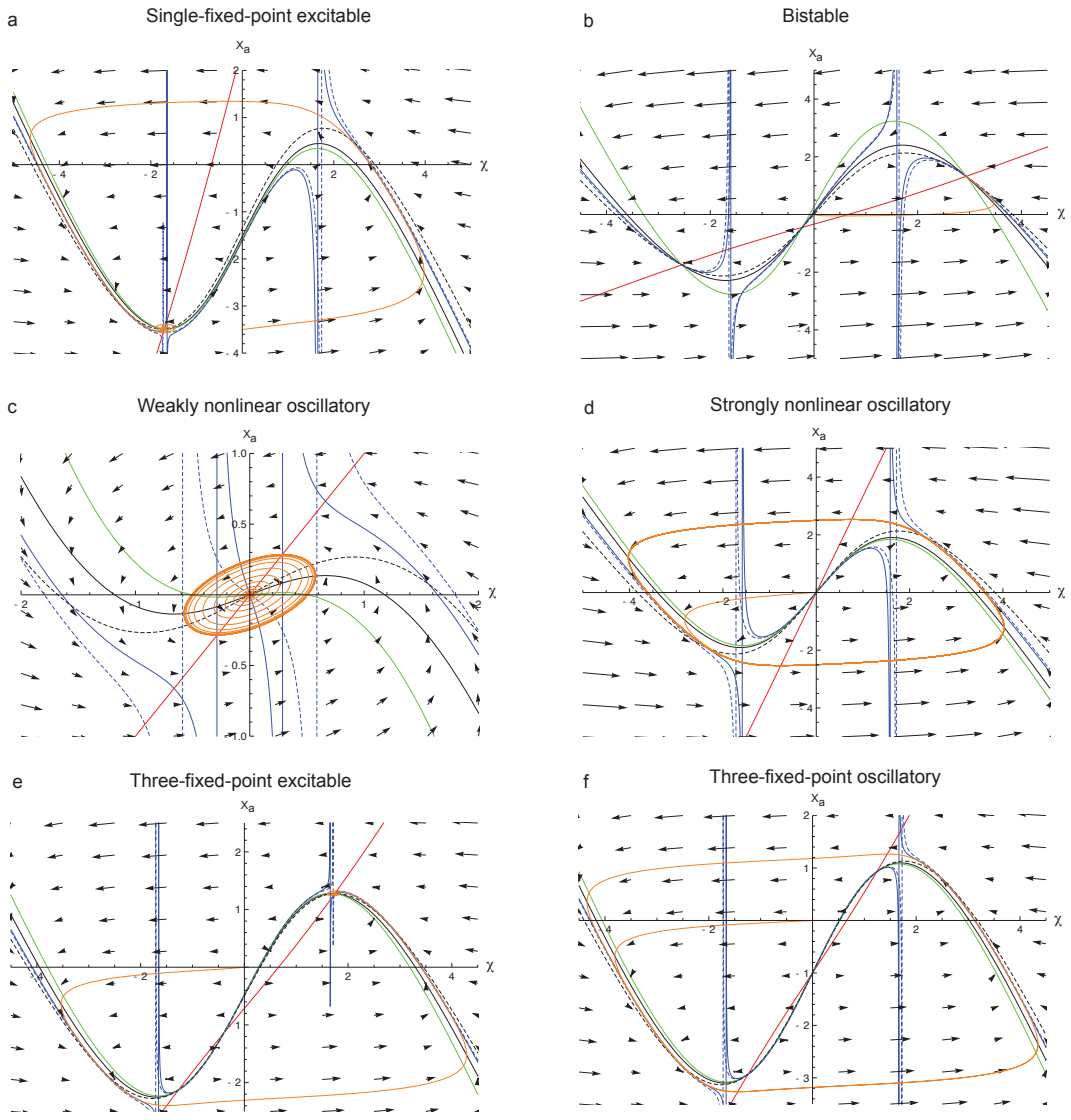

Figure 3.1: *Dynamical regimes of the hair bundle*
Phase portraits in the (χ, X_a)-plane corresponding to simulation of equation (2.1), in various dynamical regimes. The legend for this figure is given in Table 3.1. The parameter values are given in Table 3.2. a) Single-fixed-point excitable regime; b) Bistable regime; c) Weakly nonlinear oscillatory regime; d) Relaxation oscillation regime; e) Three-fixed-point excitable regime; f) Three-fixed-point oscillatory regime

Parameter regime	ε	η	η_a	κ	κ_a	C
a. Single-fixed-point excitable	0.05	8	2	0.5	0.4	-4.68
b. Bistable	0.05	8	-1	0.5	1.5	-4
c. Weakly nonlinear oscillatory	0.1	4.9	0	0.5	1	-2.45
d. Relaxation oscillation	0.1	8	0	0.5	0.3	-4
e. Three-fixed-point excitable regime	0.05	8	-1	0.6	0.7	-4.3
f. Three-fixed-point oscillatory regime	0.05	8	-1	0.5	0.5	-4.5

Table 3.2: *Parameter values for Figure 3.1 depicting the model's dynamical regimes.*

Figure 3.2 illustrates saddle-node, super-critical Hopf, and sub-critical Hopf bifurcations of fixed points.

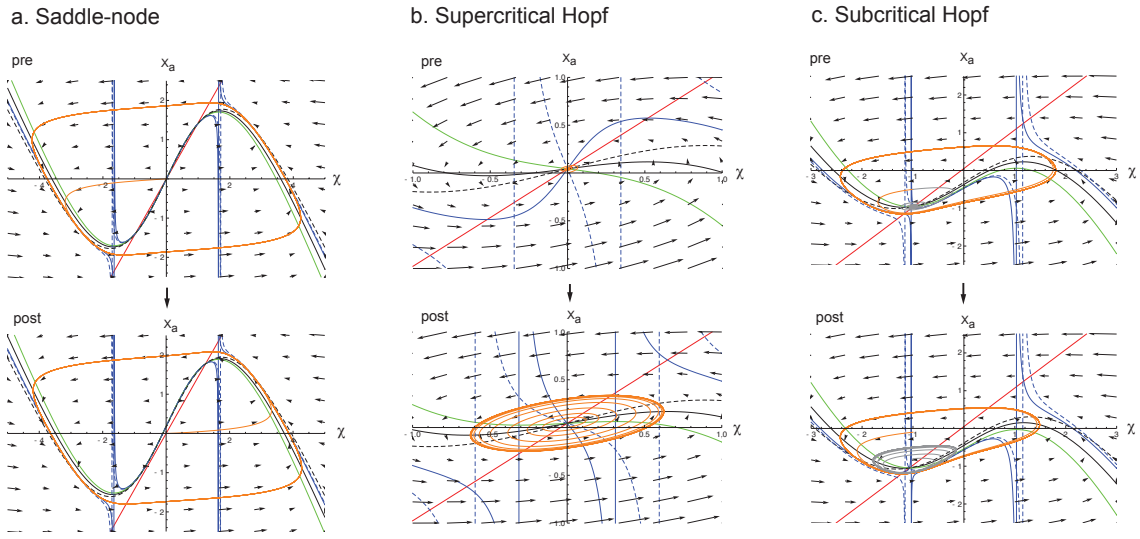

Figure 3.2: *Bifurcations of fixed points*
a. Saddle-node bifurcation b) supercritical Hopf bifurcation. c.) Sub-critical Hopf bifurcation.The legend for this figure is given in Table 3.1.

For the Pade-approximated model described above, we can calculate analytically the entire codimension-1 bifurcation structure (i.e.: the bifurcations involving variation of a single parameter) in all parameter regimes. Specifically, we can calculate the fixed points, eigenvalues, normal-form coefficients, and conditions for bifurcation of the model in all parameter regimes.

3.1 Bifurcations of fixed points

3.1.1 Calculation of fixed-point coordinates

The system's fixed points χ^* satisfy:

$$F_{elastic}(\chi^*) = \varepsilon(\kappa + \kappa_a)\chi^* - \varepsilon(\eta\kappa_a - \eta_a\kappa)p_o(\chi^*) - \varepsilon\kappa_a C = 0 \qquad (3.1)$$

We can determine the fixed points $(\chi^*, N_\chi(\chi^*))$ of the Pade-approximated system exactly by the solving the rational equation

$$N_\chi(\chi^*) - N_a(\chi^*) = 0 \qquad (3.2)$$

corresponding to the condition that the velocities of χ and X_a vanish. Alternatively, we can construct the order (3,2) Pade approximation of $F_{elastic}$ (which we call $F_{e,P}$)

$$F_{e,P} = -\omega_\kappa^2 \chi + \frac{\omega_\kappa^2 d_\kappa}{24} \chi \left(1 + \frac{50}{10 + \chi^2}\right) + \left(\varepsilon \kappa_a C_{static} + \frac{\omega^2 d_\kappa}{2}\right) \qquad (3.3)$$

and solve for its roots, which satisfy the cubic equation:

$$F_{e,0} - k_0 \chi + \frac{1}{10}\chi^2 - \frac{1}{10}\left(\omega_\kappa^2 - 2k_{nl}\right)\chi^3 = 0 \qquad (3.4)$$

where

$$F_{e,0} = F_{elastic}(0) = \varepsilon \kappa_a C + \frac{1}{2}\omega_\kappa^2 d_\kappa \quad , \quad k_0 = Det_A(0) = \omega_\kappa^2 - \frac{1}{4}\omega_\kappa^2 d_\kappa \quad , \quad k_{nl} = \frac{1}{48}\omega_\kappa^2 d_\kappa \qquad (3.5)$$

Thus, the Pade-approximated model admits generically either three fixed points, corresponding to case of three real roots, or a single fixed point, corresponding to the case of a single real root and a pair of complex conjugate roots.

The eigenvalues λ_+ and λ_- of the Jacobian A are determined by Tr_A and Det_A according to the equation:

$$\lambda_\pm = \frac{Tr_A}{2} \pm \frac{1}{2}\sqrt{Tr_A^2 - 4Det_A} \tag{3.6}$$

Substituting the approximate solution for a fixed point into equation (3.6) gives an approximate solution for the eigenvalues of A at the fixed point χ^* .

3.1.2 Saddle-node bifurcation

Two kinds of co-dimension-1 bifurcations of a fixed point can occur in the hair-bundle model (and in two-dimensional dynamical systems generally): a saddle-node bifurcation and a Hopf bifurcation.

At a saddle-node bifurcation, two fixed points collide and disappear. The eigenvalues of the jacobian A at each fixed point approach zero, and past the bifurcation, the fixed point disappears. At the bifurcation point, the $F_{elastic}$ function is non-monotone.

The condition for a repeated root (and hence two fixed points) is that the discriminant of the cubic equation (3.4) vanish:

$$\frac{1}{500}\left(-135F_{e,0}^2\left(\omega_\kappa^2-2k_{nl}\right)^2-2F_{e,0}\left(1-90k_0\left(\omega_\kappa^2-2k_{nl}\right)\right)+5k_0^2(1-80k_0\left(\omega_\kappa^2-2k_{nl}\right)\right) \tag{3.7}$$

This corresponds to the condition for a saddle-node bifurcation in the model. This condition is cubic in k_0, and quadratic in ω_κ^2, F_{e_0}, and k_{nl}; thus, fixing any three of these parameters, the value of the fourth parameter at which a saddle-node bifurcation (if it exists) occurs can be determined analytically by checking for real solutions.

Equivalently, the saddle-node bifurcation occurs in the Pade-approximated model when a real root of the fixed-point equation (3.4) also satisfies, $Det_{A,P} = 0$:

$$-1+\omega_\kappa^2 d_\kappa\frac{(600-30\chi^2+\chi^4)}{24(10+\chi^2)^2}=0 \tag{3.8}$$

whose solutions are the roots of $\frac{d}{d\chi}F_{e,P}$.

3.1.3 Hopf bifurcation

At a Hopf bifurcation, the matrix A at the fixed point admits a pair of complex-conjugate eigenvalues whose real parts transition from negative to zero at the bifurcation. Past the bifurcation, the fixed point becomes unstable, and the system tends toward a limit cycle. At the Hopf bifurcation, the $F_{elastic}$ curve is monotone.

An approximate analytic condition for a Hopf bifurcation at a fixed point in the simplified model is that the order-(3,2) Pade-approximated function $Tr_{A,P}$ of Tr_A vanish at a fixed point, while Det_A remains non-negative. This occurs when a real solution to the approximate fixed-point equation (3.4) also satisfies both the equation corresponding to $Tr_{A,P} = 0$ and the inequality corresponding to $Det_{A,P} \geq 0$:

$$-(1 + \varepsilon + \varepsilon\kappa_a) + \alpha_\varepsilon \frac{(600 - 30\chi^2 + \chi^4)}{24(10 + \chi^2)^2}) = 0 \tag{3.9}$$

$$-1 + \omega_\kappa^2 d_\kappa \frac{(600 - 30\chi^2 + \chi^4)}{24(10 + \chi^2)^2} \geq 0 \tag{3.10}$$

3.1.4 Bogdanov-Takens instability

Finally, for the Pade-approximated model, the condition for a codimention-2 Bogdanov-Takens instability, in which a saddle-node and Hopf bifurcation occur concurrently (i.e.: the bifurcating fixed point has two zero eigenvalues), is that a real root of the fixed-point equation (3.4) satisfy both (3.8) and (3.9), the conditions for a saddle-node and a Hopf bifurcation, respectively.

3.1.5 Physical interpretation of bifurcation conditions

In physical terms, tuning to the critical point of a *Hopf* bifurcation corresponds to the condition that at the fixed point χ^*, the effective drag coefficient μ vanish, while the effective stiffness k_e remain positive (i.e.: the effective elastic force remain restorative):

$$\mu(\chi^*) = 0 \quad , \quad k_e(\chi^*) > 0 \tag{3.11}$$

The condition for a *saddle-node* bifurcation is that

$$k_e(\chi^*) = 0 \tag{3.12}$$

The condition $\mu(\chi^*) = 0$ is equivalent to the critical slipping condition in equation (2.59) above. Similarly, $k_e(\chi^*) = 0$ is equivalent to the critical buckling condition in equation (2.60).

$$-\left(\frac{d\phi}{d\chi}\right)_{\chi=\chi^*} = \frac{\mu_\infty}{\alpha_{\varepsilon,slipping}} \tag{3.13}$$

Thus, the slipping and buckling conditions give precise biophysical interpretations for the conditions for a Hopf and saddle-node bifurcation.

3.1.6 Bifurcations of limit cycles

Just as the system's fixed points appear, disappear, and change stability as parameters of the system are varied, so too do its limit cycles. We have already seen the birth of limit cycles by a super-critical Hopf bifurcation. Here we describe two other mechanisms by which limit cycles change; the saddle-homoclinic bifurcation and the fold bifurcation. Figure 3.3 shows examples of each of these bifurcations.

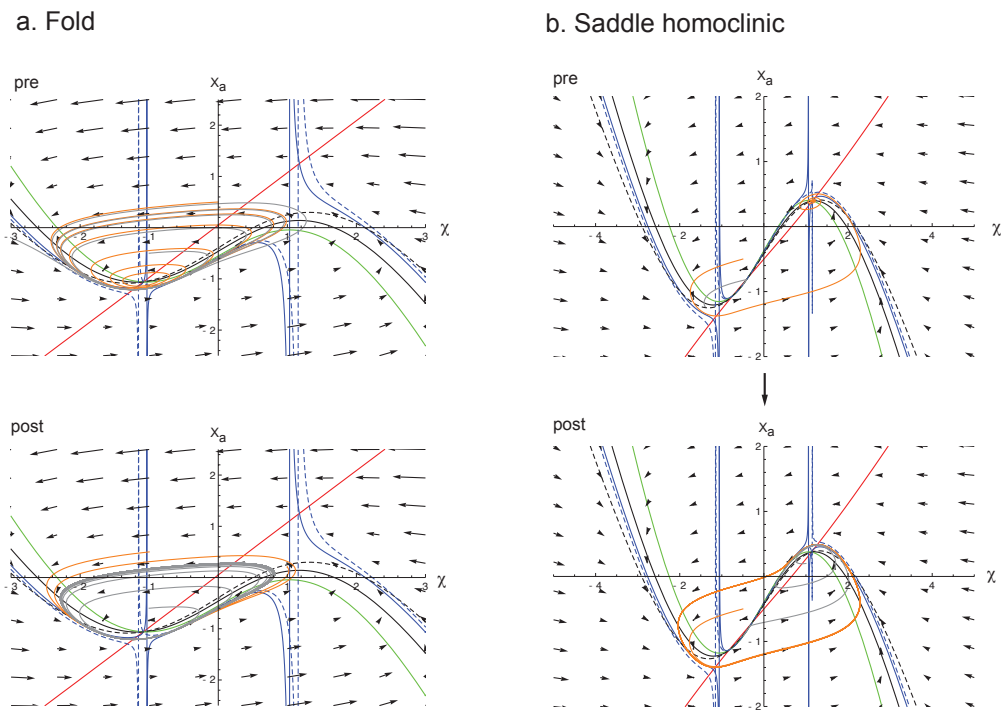

Figure 3.3: *Bifurcations of limit cycles*
a.) Fold bifurcation b) Big-saddle homoclinic bifurcation. The legend for this figure is given in Table 3.1.

3.1.7 Homoclinic bifurcation

At a saddle homoclinic bifurcation, a homoclinic orbit emanating from a saddle node gives rise to a limit cycle as a parameter of the system is tuned. Close to the big-saddle homoclinic bifurcation seen in simulations of the hair-bundle model, the period of the limit cycle is dominated by the time spent by the system near the saddle node; accordingly the unstable eigenvalue of the saddle node gives a reasonable estimate of the frequency of oscillation.

Fold bifurcation

In the fold bifurcation, a pair of limit cycles –one stable and one unstable– appear, with the stable limit cycle surrounding the unstable one. The Poincare section of the saddle homoclinic orbit undergoes a saddle-node bifurcation. As the bifurcation parameter is tuned, the unstable limit cycle shrinks until it coallesces with the stable fixed point it encloses. This fixed point undergoes a subcritical Hopf bifurcation, losing its stability, and the system jumps abruptly to a finite amplitude limit-cycle oscillation.

Chapter 4

Spontaneous oscillations of the hair bundle

The saccular hair-bundle operates at low Reynold's number. For objects of its size, viscosity overwhelms inertia, precluding even damped oscillations in the absence of an active mechanism. The hair bundle's active process counteracts both the viscous damping of the bundle due to hydrodynamic drag and the molecular friction due to interactions between the motors and the actin cores. If sufficiently powerful, the active process can overcome linear damping altogether; the hair bundle will begin to oscillate spontaneously, and its fixed point will become unstable to small perturbations.

In this section, we study by asymptotic methods the dynamics of the hair bundle in the weakly nonlinear and strongly nonlinear single-fixed-point regimes. For simplicity of exposition, we confine our analysis to the case in

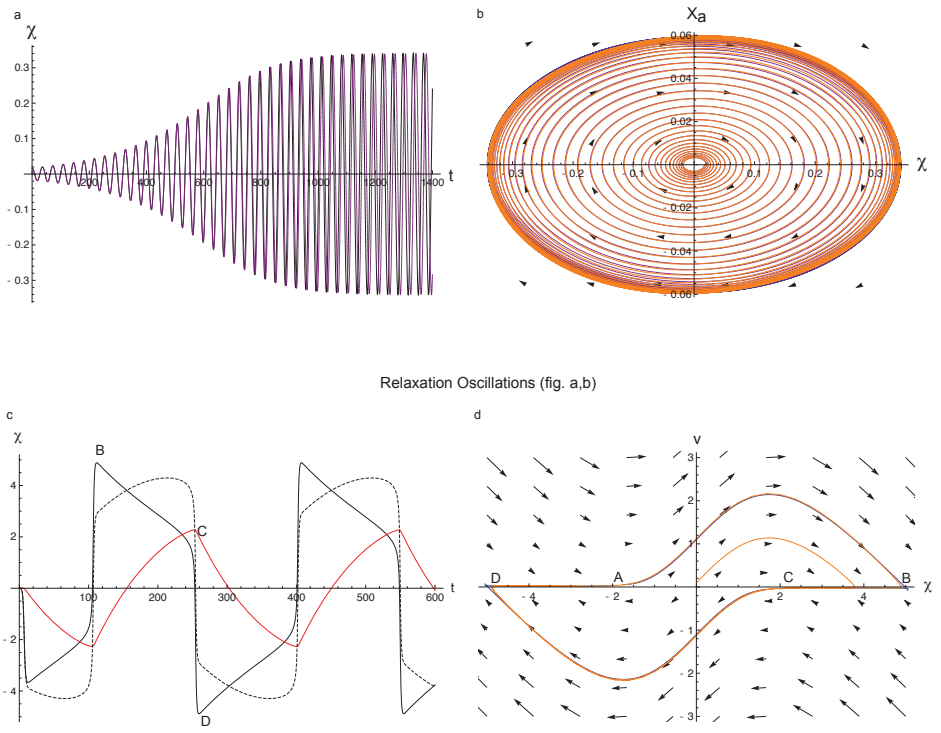

Figure 4.1: *Nonlinear oscillations of the hair bundle*
Trajectories and phase portrait for the simplified model in the weakly nonlinear (a,b) and strongly nonlinear (c,d) oscillatory regimes. a), b) *Weakly nonlinear oscillations.* Shown in black is the numerical solution to equation (2.1), for the parameter regime: ($\varepsilon = 0.1$, $\eta = 4.84374$, $\eta_a = 0.087394$, $\kappa = 0.5$, $\kappa_a = 1$ $C = -2.4$). Shown in purple, the multiple-scales solution (given by equation (4.34)) for the same parameter values and initial conditions. The ellipse in blue in b) depicts the approximate limit cycle described by equation (4.36). c), d) *Strongly nonlinear oscillations.* Trajectory (c) and phase portrait (d) for the simplified model undergoing relaxation oscillations. Parameter values for the relaxation oscillation parameter regime: ($\varepsilon = 0.01$, $\eta = 8$, $\eta_a = 0$, $\kappa = 0.5$, $\kappa_a = 0.5$, $C = -6$). Shown in orange in figure d), the integral curve calculated by numerical simulation of the simplified model; In blue, the approximation to the integral curves calculated by boundary-layer methods. The blue curves joining in D to A, B to C correspond to the outer solution given by equation (4.57). The blue curves joining A to B, C to D correspond to approximate solutions given by the inner equation (4.91). The portion of the orange curve emanating from near the origin corresponds to the transient approach to the limit cycle. Boundary-layer calculations in the oscillatory regime yields $T_{AB} = T_{CD} \cong 6.7$, $T_{DA} = T_{BC} \cong 127.9$, and an estimated amplitude $A \cong 4.2$.

which the open probability p_o^* at the fixed point χ^* is $1/2$, corresponding to $\chi^* = 0$. More precisely, we assume that:

$$C \equiv \frac{\eta\kappa_a - \kappa\eta_a}{2\kappa_a} = \frac{\omega_\kappa^2 d_\kappa}{2\varepsilon\kappa_a} \tag{4.1}$$

Under this assumption, the phenomenological equation (2.55) reduces to:

$$\frac{d^2\chi}{dt^2} + (1 + (\varepsilon(1+\kappa_a))\frac{d\chi}{dt} + \omega_\kappa^2\chi = \alpha_\varepsilon\phi(1-\phi)\frac{d\chi}{dt} - \omega_\kappa^2 d_\kappa\left(\phi - \frac{1}{2}\right) \tag{4.2}$$

In the weakly nonlinear oscillatory regime in the vicinity of a Hopf bifurcation, the method of multiple scales yields an approximate analytic description of both the rapid sinusoidal dynamics of the phase and the slow monotonic dynamics of the amplitude of the bundle's trajectory. In the strongly nonlinear oscillatory regime boundary-layer analysis gives a uniform approximation to the bundle's limit cycle.

4.1 Weakly nonlinear regime

4.1.1 Heuristic analysis

The weakly nonlinear regime is characterized by a small effective damping term. Taylor expansion of the phenomenological equation about $\chi^* = 0$ yields as an approximate description the *van der Pol-Duffing equation*:

$$\frac{d^2\chi}{dt^2} + \left[\mu_0 + \mu_{nl}\chi^2\right]\frac{d\chi}{dt} + k_0\chi + k_{nl}\chi^3 + O(\chi^3) = 0 \tag{4.3}$$

$$\mu_0 =_{df} \mu(0) = 1 + \varepsilon + \varepsilon\kappa_a - \frac{\alpha_\varepsilon}{4} \qquad \mu_{nl} = \frac{1}{2}\frac{d^2\mu}{d\chi^2}|_{\chi=0} =_{df} \frac{\alpha_\varepsilon}{16} \tag{4.4}$$

$$k_0 = k_e(0) = \omega_\kappa^2(1 - \frac{d_\kappa}{4}) \quad , \quad k_{nl} = \frac{1}{2}\frac{d^2k_e}{d\chi^2}|_{\chi=0} = \frac{\omega_\kappa^2 d_\kappa}{48} \tag{4.5}$$

As in the van der Pol equation, the nonlinear dissipation coefficient $\mu_0 + \mu_{nl}\chi^2$ depends quadratically on χ. It will assume negative values (arising from the injection of energy by the active process) provided μ_0 is negative, and will assume positive values for sufficiently large excursions in χ, provided μ_{nl} is positive. As in the Duffing equation, the elastic force $-k_0\chi - k_{nl}\chi^3$ has both a linear and cubic dependence on the state variable χ, and will be restorative near the fixed point provided k_0 is positive.

Thus, assuming μ_{nl} and k_0 positive, the system passes through a supercritcal Hopf bifurcation as the parameter μ_0 is varied. For $\mu_0 > 0$, the system is linearly damped. At $\mu_0 = 0$, the system is poised at the supercritical Hopf bifurcation; the eigenvalues of the linearized system are purely imaginary. For $\mu_0 < 0$, the linear term in $\frac{d\chi}{dt}$ is explosive; the growth of bundle's amplitude of movement is restricted by the nonlinear dissipative term $\mu_{nl}\chi^2\frac{d\chi}{dt}$; and, since the effective elastic force is restorative, the system oscillates spontaneously.

Three time-scales appear in the oscillatory regime past the supercritical Hopf bifurcation: i) a fast time-scale of oscillation $O(k_0^{-1/2})$ on which the system undergoes nearly sinusoidal oscillations; ii) a slow time-scale $O(\mu_0^{-1})$ on which the amplitude of oscillation approaches the limit-cycle amplitude. iii) an ultra-slow time-scale on which the phase shift varies due to the nonlinear elastic term.

Near the Hopf bifurcation the dynamics of the phase and of the amplitude are approximately independent of one another. A clear indication that this is the case appears in the analytic solution to the transient dynamics of the under-damped (i.e.: $\mu_0 > 0$) van der Pol-Duffing system, linearized about the fixed point $\chi^* = 0$:

$$\chi(t) = \chi(0)\exp\left[-\frac{1}{2}\mu_0 t\right]\cos\left(\left(k_0 - \left(\frac{\mu_0}{2}\right)^2\right)^{1/2} t + \phi_0\right) \qquad (4.6)$$

We observe, in equation (4.6), that the amplitude $|A|$ of the damped oscillations decays on a time-scale $O(\mu_0)$, independent of the parameter k_0:

$$|A| = \chi(0) \exp[-\frac{1}{2}\mu_0 t] \tag{4.7}$$

and, provided $\mu_0 \ll k_0^{-1/2}$, the phase varies with a frequency $O(\sqrt{k_0})$, approximately independent of the parameter μ_0.

By analogy to the linearized dynamics, we expect that in the oscillatory regime near the Hopf bifurcation, the rapid phase dynamics will proceed nearly sinusoidally, with the frequency $\sim \sqrt{k_0}$:

$$\chi \sim |A| \cos(\sqrt{k_0} t) \tag{4.8}$$

The growth or decay of the amplitude $|A|$ will take place on the slow time-scale set by μ_0, where, by assumption, $\mu_0 k_0^{1/2} \ll 1$. Since the viscous terms in μ_0 and μ_{nl} control the dynamics of $|A|$, we expect the equation describing the evolution of $|A|$ to imply:

$$\beta \frac{d|\tilde{A}|}{d(\mu_0 t)} \sim \beta|\tilde{A}| - \left(\frac{\mu_{nl}}{\mu_0}\right)\beta^3|\tilde{A}|^3 \tag{4.9}$$

where β is a function of the parameter μ_0 that vanishes as μ_0 tends to zero (corresponding to the contraction and disappearance of the limit cycle as $\mu_0 \to 0^-$) and $|\tilde{A}|$ is the amplitude of oscillation normalized to the amplitude of the limit cycle.

$$|A| = \beta|\tilde{A}| \tag{4.10}$$

$$\lim_{\mu_0 \to 0} \beta = 0 \tag{4.11}$$

To determine β, observe that the limit-cycle amplitude $|A|_{s.s.}$ is reached when the explosive linear term balances the non-linear dissipative term:

$$-\mu_0 \beta \left|\tilde{A}\right|_{s.s.} \sim \mu_{nl}\beta^3 \left|\tilde{A}\right|^3_{s.s.} \tag{4.12}$$

whence:

$$\beta \left| \tilde{A} \right|_{s.s.} \sim \sqrt{\frac{-\mu_0}{\mu_{nl}}} \tag{4.13}$$

Choosing

$$\beta = \sqrt{\frac{-\mu_0}{\mu_{nl}}} \tag{4.14}$$

scales $\tilde{A}$ to the limit-cycle amplitude:

$$\chi \sim \sqrt{\frac{-\mu_0}{\mu_{nl}}} |\tilde{A}(\mu_0 t)| \cos(\sqrt{k_0} t) \tag{4.15}$$

Finally, in view of the relation (4.9), whose corresponding ordinary differential equation has an analytic solution, we expect the trajectory of χ to satisfy:

$$\chi \sim \sqrt{\frac{-\mu_0}{\mu_{nl}}} \left[\frac{\exp\left(-\frac{1}{2}\mu_0 t\right)}{\sqrt{\exp\left(-\mu_0 t\right) - 1 + \rho_0^{-2}}} \right] \cos(\sqrt{k_0} t) \tag{4.16}$$

4.1.2 Multiple-scales analysis

The multiple-scales procedure renders explicit the hypothesis that the dynamics in the weakly nonlinear regime are determined through effectively independent processes unfolding concurrently on several time-scales. the procedures replaces the single time variable t in an ordinary differential equation with separate time variables t_1, t_2, etc. that are treated as independent of one another. Correspondingly, the original ordinary differential equation in t is replaced by a partial differential equation in the variables t_1, t_2, etc. Perturbation of this partial differential equation generates a hierarchy of equations whose solutions, when subject to the requirement that secular terms (i.e.: terms diverging in time) vanish, together provide a uniform approximation to the original dynamical equation.

Motivated by the heuristic analysis in section (4.1.1) above, we introduce the perturbation parameter ε_p; a time variable t_p corresponding to t rescaled by the period $k_0^{-1/2}$ of the limit cycle; and appropriate rescalings of the system's parameters:

$$\varepsilon_p =_{df} \frac{-\mu_0}{\mu_{nl}} = \left(\frac{\mu_f - \alpha_{\varepsilon,slipping}}{\mu_f} \right) \tag{4.17}$$

$$t_p =_{df} \sqrt{k_0}t \tag{4.18}$$

$$\mu_{0,p} = \frac{\mu_0}{\sqrt{k_0}} \quad , \quad \mu_{nl,p} = \frac{\mu_{nl}}{\sqrt{k_0}} \quad , \quad k_{nl,p} = \frac{k_{nl}}{k_0} \tag{4.19}$$

Having introduced a rescaling of the parameters and of the independent variable, we seek, next, a rescaling of χ that casts the dynamical equations into the scaled form:

$$\frac{d^2\chi_p}{dt_p^2} + \chi_p = \varepsilon_p \; f_p\left(\chi_p, \frac{d\chi_p}{dt_p}\right) \tag{4.20}$$

$$f_p\left(\chi, \frac{d\chi_p}{dt_p}\right) =_{df} -\mu_{nl,p}(1+\chi_p^2)\frac{d\chi_p}{dt_p} + k_{nl,p}\chi_p^3 \tag{4.21}$$

where ε_p and f_p satisfy the scaling assumptions characteristic of the *weakly nonlinear* regime:

$$\varepsilon_p \ll 1 \quad , \quad f_p = O(1) \tag{4.22}$$

To this end, we define the rescaled extension variable χ_p:

$$\chi_p =_{df} \frac{\chi}{\beta} \tag{4.23}$$

in terms of the variable χ and an unspecified amplitude factor $\beta \equiv \beta(\varepsilon_p)$ whose asymptotic dependence upon ε_p we determine by dominant balance. Since the limit cycle vanishes as $\varepsilon_p \to 0$, we require, minimally, that:

$$\lim_{\varepsilon_p \to 0} \beta(\varepsilon_p) = 0 \tag{4.24}$$

Substituting (4.23) into (4.20) gives:

$$\beta = \varepsilon^{1/2} \tag{4.25}$$

With β now specified, we posit the perturbation expansion:

$$\chi_p = \chi_{p,0} + \varepsilon_p \chi_{p,1} + O(\varepsilon_p^2) \tag{4.26}$$

and introduce the slow time-scale τ_p:

$$\tau_p =_{df} \varepsilon_p t \tag{4.27}$$

We are now in a position to apply the multiple scales procedure; we assume that the variables χ_p, $\chi_{p,0}$, $\chi_{p,1}$, ... are functions of both t and τ_p; accordingly, we replace the ordinary derivatives in the dynamical equation with partial derivatives in the variables t and τ_p:

$$\frac{d}{dt} = \frac{\partial}{\partial t} + \varepsilon \frac{\partial}{\partial \tau_p} \tag{4.28}$$

With these substitutions, we obtain a hierarchy of perturbation equations whose solutions give estimates of the phase and amplitude dynamics. The $O(1)$ and $O(\varepsilon_p)$ perturbation equations are:

$$O(1): \qquad \frac{\partial \chi_{p,0}}{\partial t} + \chi_{p,0} = 0 \tag{4.29}$$

$$O(\varepsilon_p): \qquad \frac{\partial^2 \chi_{p,1}}{\partial t^2} + \chi_{p,1} = -2\frac{1}{\partial \tau_p}\left(\frac{\partial \chi_{p,0}}{\partial t}\right) + f_p(\chi_{p,0}) \tag{4.30}$$

Solving the $O(1)$ equation for $\chi_{p,0}$ gives:

$$\chi_{p,0} = A\left(\tau_p\right) exp\left(i\sqrt{k_0}t\right) + A^*\left(\tau_p\right) exp\left(-i\sqrt{k_0}t\right) \tag{4.31}$$

Substituting this solution for $\chi_{p,0}$ into the $O(\varepsilon_p)$ equation, and enforcing the requirement that secular terms vanish, yields a differential equation in the complex amplitude function $A(\tau_p)$, of modulus ρ and argument θ:

$$\frac{dA}{d\tau_p} = \frac{1}{2}A + \left(i\frac{3}{2}k_{nl} - \frac{\mu_{nl}}{2}\right)|A|^2 A \tag{4.32}$$

$$A = \rho(\tau_p)\exp[\theta(\tau_p)] \tag{4.33}$$

The dynamical equation for ρ derived from the amplitude equation (4.32) can be solved analytically, by noting that the equation for $2\rho\frac{d\rho}{dt}$ is a logistic equation. The corresponding solution in terms of χ vindicates the heuristic analysis that led to equation (4.16), and is given by:

$$\chi(t) = 2\left(\frac{-\mu_0}{\mu_{nl}}\right)^{1/2}\left[\frac{\exp\left(-\frac{1}{2}\mu_0 t\right)}{\sqrt{\exp\left(-\mu_0 t\right) - 1 + \rho_0^{-2}}}\right] cos\left(\sqrt{k_0}t + \phi_0\right) \quad (4.34)$$

where ρ_0 and ϕ_0 set, respectively, the initial amplitude and phase of the system according to:

$$(\chi(0), v(0)) = (\rho_0 \cos(\phi_0), \rho_0 \sin(\phi_0)) \quad (4.35)$$

We see from this solution that the limit cycle in the (χ, v)-plane is an ellipse described by:

$$\left(\frac{\chi}{2\sqrt{-\mu_0\mu_{nl}^{-1}}}\right)^2 + \left(\frac{v}{2\sqrt{-k_0\mu_0\mu_{nl}^{-1}}}\right)^2 = 1 \quad (4.36)$$

or, equivalently, by the total-energy equation:

$$\frac{1}{2}k_0\chi_{l.s.}^2 + \frac{1}{2}v_{l.s.}^2 = -2k_0\mu_0\mu_{nl}^{-1} \quad (4.37)$$

Figure 4.1 shows that the perturbative solutions given by (4.34)-(4.36) are in close agreement with the solution calculated by numerical integration of equation (2.1). As discussed in the section (4) of the supplementary material, for the choice of parameters that puts the operating point at $\chi = 0$ as in this example, the multiple scales solution agrees exactly with the normal form approximation.

4.2 Strongly nonlinear regime

Saccular hair bundles whose active movements have been characterized *in vitro* appear to operate far from the Hopf bifurcation; they typically exhibit relaxation oscillations characteristic of a strong nonlinearity. Presently, we derive from the simplified model, using boundary-layer analysis, an explanation for the biophysical mechanisms underlying these oscillations.

We again assume for simplicity (as in equation (4.1) above) that the dynamical equation is symmetric about an unstable fixed point at $\chi = 0$. We make the additional simplifying assumption regarding the motor nonliearity parameter η_a, that:

$$\eta_a \equiv 0 \tag{4.38}$$

This condition (or, equivalently, the condition $\phi_{u,max} = Sf_m = \eta$) corresponds to the circumstance in which the change in the elastic force upon the adaptation complex due to gating of the transduction channels is just balanced by the Ca^{2+}-induced change, opposite in sign, in the climbing force generated by the adaptation motors.

Strong nonlinearity refers to any condition in which the highest-order derivative (in the case at hand, the acceleration term in χ) is multiplied by a small parameter. Consider, for instance, $\varepsilon_p = \frac{-\mu_0}{\mu_{nl}}$ introduced in the multiple-scales analysis above. If $\varepsilon_p^{-2} \ll 1$, then the change of time variable $t_1 = \frac{t}{\varepsilon_p}$ shows that this condition gives rise to a strong nonlinearity. Below, on the observation that the time-scale parameter ε is a natural small parameter of the simplified model, we consider another strongly nonlinear regime, characterized by the assumption:

$$\varepsilon \ll 1 \tag{4.39}$$

Accordingly, the asymptotic relations for the boundary-layer analysis presented in this section hold in the limit $\varepsilon \to 0$.

In the strongly nonlinear regime, the system can undergo relaxation oscillations, in which its trajectory alternates between slow *outer* phases of motion (scaled to be of duration $\sim O(1)$) and fast *inner* phases of motion (of duration $\sim O(\varepsilon)$). Between the outer and inner phases, the system passes through a *transition* phase of intermediate duration $\sim O(\varepsilon^{2/3})$.

To carry out the boundary-layer analysis, we introduce for each of the outer, transition, and inner layers, appropriate time-scales on which to examine the dynamics. From a consideration of the dominant balance among the elastic, viscous, and inertial forces, we obtain approximations for the dynamics in each layer that match asymptotically the approximations constructed for adjacent layers. Piecing together the approximations for the limit cycle's succession of layers yields a uniform approximation to the system's course through the state space.

We define the outer time variable τ, the transition time variable t_{tr} and the inner time variable t_{in} by:

$$\tau =_{df} \varepsilon t \quad , \quad t_{tr} =_{df} \varepsilon^{-2/3} t \quad , \quad t_{in} = t = \varepsilon^{-1} t \tag{4.40}$$

With respect to the outer time variable τ, which will serve as the ref-

erence (i.e.: O(1)) time variable for the boundary-layer analysis, the phenomenological equation assumes the form:

$$\varepsilon\frac{d^2\chi}{d\tau^2}+\left[1+\varepsilon(1+\kappa_a)-\frac{\eta}{4}\right]\frac{d\chi}{d\tau}+(\kappa+\kappa_a)\chi-\eta\ \kappa_a\ \left(p_o-\frac{1}{2}\right)=0 \quad (4.41)$$

or, separated into effective active and passive terms:

$$\varepsilon\frac{d^2\chi}{d\tau^2}+[1+\varepsilon(1+\kappa_a)]\frac{d\chi}{d\tau}+(\kappa+\kappa_a)\chi=-\eta\left[\frac{d\phi}{d\tau}+\kappa_a\left(\phi-\frac{1}{2}\right)\right] \quad (4.42)$$

We see from equation (4.41) that the acceleration term is multiplied by the small parameter ε, and so the system is, indeed, strongly nonlinear.

The points A, B, C, and D delimiting the inner, transition, and outer layers of the trajectory are illustrated in Figure 4.1, and their coordinates are given by:

$$A =_{df} (\chi_A, X_{aA}), B =_{df} (\chi_B, X_{aB}), C =_{df} (\chi_C, X_{aC}), D = (\chi_D, X_{aD}) \tag{4.43}$$

$$\frac{d\Psi_\chi}{d\chi}(\chi_A) = 0 \quad , \quad \frac{d^2\Psi_\chi}{d\chi^2}(\chi_A) > 0 \tag{4.44}$$

$$\frac{d\Psi_\chi}{d\chi}(\chi_C) = 0 \quad , \quad \frac{d^2\Psi_\chi}{d\chi^2}(\chi_C) < 0 \tag{4.45}$$

$$\chi_B > 0 \quad , \quad \Psi(\chi_B) = X_{aA} \quad , \quad X_{aB} = X_{aA} \tag{4.46}$$

$$\chi_D < 0 \quad , \quad \Psi(\chi_D) = X_{aC} \quad , \quad X_{aD} = X_{aC} \tag{4.47}$$

The dependence of these coordinates upon the parameters can readily be determined analytically under the Pade approximation.

4.2.1 Outer phase $\sim O(1)$

During the slow outer phase, of duration $\sim O(1)$, the effective viscous and elastic forces balance one another and the acceleration of χ is negligible. More precisely, if we rescale the effective forces as well as the v-nullcline function:

$$f_{inertial} =_{df} \varepsilon^{-1} F_{inertial} \quad , \quad f_{viscous} =_{df} \varepsilon^{-1} F_{viscous} \quad , \quad f_{elastic} =_{df} \varepsilon^{-1} F_{elastic} \tag{4.48}$$

$$\psi_v =_{df} \frac{f_{elastic}}{\mu} = \frac{\Psi_v}{\varepsilon} \tag{4.49}$$

then the dominant-balance relations for the outer layer are:

$$f_{inertial} \ll f_{viscous} \sim f_{elastic} \sim 1 \tag{4.50}$$

To obtain the outer approximation, let us perturb the force-balance equation (4.41) in ε. To accomplish this, we first introduce perturbation expansions for the state variables χ and X_a:

$$\chi = \chi_0 + \varepsilon\chi_1 + O(\varepsilon^2) \tag{4.51}$$

$$X_a = X_{a,0} + \varepsilon\chi_1 + O(\varepsilon^2) \tag{4.52}$$

The drag coefficient μ, the $v-$nullcline function Ψ_v, and the elastic force $f_{elastic}$, will then have the corresponding perturbation expansions:

$$\mu(\chi) = \tilde{\mu}_0 + \varepsilon\ \tilde{\mu}_1 + O(\varepsilon^2) \tag{4.53}$$

$$\Psi_v(\chi) = \Psi_{v,0} + \varepsilon\ \Psi_{v,1} + O(\varepsilon^2) \tag{4.54}$$

$$f_{elastic}(\chi) = f_{elastic,0} + \varepsilon\ f_{elastic,1} + O(\varepsilon^2) \tag{4.55}$$

where we have used tildes, where necessary, to distinguish terms in the perturbation expansions from constants defined previously.

Substituting the expansions (4.51)-(4.53) into the dynamical equation (4.41), we see that, to leading order, the system crawls in the outer layer at approximately the ($\chi-$ dependent) "terminal velocity" described by the leading-order term of the rescaled $v-$nullcline $\psi_{v,0}$:

$$\tilde{\mu}_0 \frac{d\chi_0}{d\tau} = f_{elastic,0} \tag{4.56}$$

or, equivalently,

$$\frac{d\chi_0}{d\tau} = \psi_{v,0}(\chi_0) \tag{4.57}$$

Integrating the outer equation (4.57) by separation of variables gives the durations T_{DA} and T_{BC} of the outer portions of the limit cycle:

$$T_{BC} = \int_{\chi_B}^{\chi_C} \frac{1}{\psi_{v,0}(\chi')} d\chi' \quad , \quad T_{DA} = \int_{\chi_D}^{\chi_A} \frac{1}{\psi_{v,0}(\chi')} d\chi' \tag{4.58}$$

T_{DA} and T_{BC} are, respectively, the duration of the relaxed (or *down*) and excited (or *up*) phases of the relaxation oscillations.

An approximation consistent with the preceding analysis emerges if we instead carry out the boundary-layer calculations with respect to the state variables χ and X_a. Rescaling to the outer time variable τ the dynamical equation (2.1) for the extension-resetting form, we obtain:

$$\varepsilon \frac{d\chi}{d\tau} = (\kappa - \varepsilon\kappa_a)\,(\Psi_\chi - X_a) \tag{4.59}$$

$$\frac{dX_a}{d\tau} = \kappa_a\,(\Psi_a - X_a) \tag{4.60}$$

Perturbing these equations in ε gives to leading order:

$$X_{a,0} = \Psi_{\chi,0}(\chi_0) \tag{4.61}$$

indicating that the system's trajectory in the (χ, X_a) phase plane approximately follows the χ nullcline. The velocity of X_a in the outer layer is given by:

$$\frac{dX_{a,0}}{d\tau} = \kappa_a \left(\Psi_{a,0} - \Psi_{\chi,0}\right) \tag{4.62}$$

The durations T_{DA} and T_{BC} of the relaxed and excited phases of oscillation are thus:

$$T_{BC} = -\int_{\chi C}^{\chi_B} \frac{1}{\left(\chi' - \Psi_{\chi,0}\left(\chi'\right)\right)} \frac{d\Psi_{\chi,0}\left(\chi'\right)}{d\chi'} d\chi' \tag{4.63}$$

$$T_{DA} = \int_{\chi D}^{\chi_A} \frac{1}{\left(\chi' - \Psi_{\chi,0}\left(\chi'\right)\right)} \frac{d\Psi_{\chi,0}\left(\chi'\right)}{d\chi'} d\chi' \tag{4.64}$$

Finally, replacing $\Psi_{\chi,0}$ with its Pade approximation N_χ gives estimates to these integrals that can be computed analytically.

As the system approaches the turning points of the function Ψ_χ (namely the points A and C), the approximate velocity $\frac{d\chi_0}{d\tau}$ diverges, marking the breakdown of the outer approximation.

4.2.2 Transition phase $\sim O(\varepsilon^{2/3})$

During the transition phases of the limit cycle, which correspond to layers encompassing the turning points A and C, the effective inertial, viscous, and elastic forces are all of comparable magnitude:

$$F_{elastic} \sim F_{viscous} \sim F_{inertial} \tag{4.65}$$

The $A \to B$ and $C \to D$ transitions, as viewed from the $O(1)$ time-scale of the outer approximation, appear discontinuous and instantaneous, as signalled by the divergence of the "terminal velocity" Ψ_v at the turning points.

To refine our account of the dynamics in the transition layers, we seek

an appropriate rescaling of the time and state variables that corresponds to the distinguished limit in which the transition solution matches asymptotically both the inner and outer solutions. To determine the properties of this limit, we first consider the $A \rightarrow B$ transition, and apply a perturbation expansion in the unspecified functions ν_1 and ν_2 of the small parameter ε, and a rescaling of time by the unspecified function ν_{tr} of ε. The precise dependence of ν_1, ν_2, and ν_{tr} upon ε we determine next by dominant balance:

$$\chi = \chi_A + \nu_1 \chi_1 + O\left(\nu_1^2\right) \quad , \quad X_a = X_{aA} + \nu_2 X_{a1} + O\left(\nu_2^2\right) \quad , \quad t_{tr} = \nu_{tr} t \tag{4.66}$$

Within the transition layer,

$$\frac{d^2\chi}{dt^2} \sim \frac{d^2(\nu_1\chi)}{d(\nu_{tr}t)^2} \quad , \quad \mu \frac{d\chi_1}{dt} \sim \left(\frac{d\mu}{d\chi}|_{\chi_A}\right) \nu_1 \chi_1 \frac{d(\nu_1\chi_1)}{d(\nu_{tr}t_1)} \quad , \quad f_{elastic} = O(1) \tag{4.67}$$

Thus,

$$\frac{\varepsilon\ \nu_1}{\nu_{tr}^2} = \frac{\nu_1^2}{\nu_{tr}} = 1 \tag{4.68}$$

from which it follows that

$$\nu_1 = \varepsilon^{1/3} \quad , \quad \nu_{tr} = \varepsilon^{2/3} \tag{4.69}$$

Near the turning points A and C, $\frac{d\chi}{dt}$ depends quadratically upon χ:

$$\frac{d\chi}{dt} = \left(\Psi_\chi\left(\chi - \chi_A\right) - X_{aA}\right) \sim \left(\chi - \chi_A\right)^2 \tag{4.70}$$

Thus, equation (4.70), along with the perturbation (4.66), gives:

$$\left(\varepsilon\nu_1\nu_2^{-1}\right)\frac{d\chi_1}{dX_{a1}} = \left(\frac{\kappa}{\chi_A - \Psi_\chi\left(\chi_A\right)}\right)\left(\frac{1}{2}N''\left(\chi_0\right)\nu_1^2\chi_1^2 - \nu_2 X_{a1}\right) \tag{4.71}$$

The matching conditions, and dominant balance, mandate a rescaling of

the state variables such that all terms in equation (4.71) are $O(1)$:

$$\varepsilon\nu_1\nu_2^{-1} = \nu_1^2 = \nu_2 \tag{4.72}$$

whence,

$$\nu_1 = \varepsilon^{1/3} \quad , \quad \nu_2 = \varepsilon^{2/3} \tag{4.73}$$

With the expansion parameters ν_1 amd ν_2 in hand, we see that to order $O(\varepsilon^{2/3})$ in the perturbation parameter ϵ, the integral curve in the (χ, X_a) phase plane is governed by the Ricatti equation (4.71) that admits a general analytic solution in terms of Airy functions. The particular solution to the Riccati equation that applies to the present case must satisfy the matching requirement that the asymptotic dynamics of the outer and inner solutions agree.

To determine this particular solution, let us first rescale equation (4.71) and the related equation for the integral curve in the vicinity of C:

$$\frac{dy_L}{dx_L} = -y_L^2 + x_L \quad , \quad \frac{dy_R}{dx_R} = -y_R^2 - x_R \tag{4.74}$$

where

$$x_L =_{df} \frac{X_a}{\psi_{xL}} \quad , \quad y_L =_{df} \frac{\chi}{\psi_{yL}} \tag{4.75}$$

$$\psi_{xL} =_{df} \frac{1}{\left(a_L^2 b_L\right)^{1/3}} \quad , \quad \psi_{yL} =_{df} \frac{1}{\left(a_L b_L^2\right)^{1/3}} \quad , \quad \psi_{xR} =_{df} \frac{1}{\left(a_R^2 b_R\right)^{1/3}} \quad , \quad \psi_{yR} =_{df} \frac{1}{\left(a_R b_R^2\right)^{1/3}} \tag{4.76}$$

$$a_L =_{df} \frac{-\kappa}{\chi_A - X_{aA}} \quad , \quad b_L =_{df} \frac{1}{2} N_\chi''(\chi_A) \quad , \quad a_R =_{df} \frac{\kappa}{\chi_C - X_{aC}} \quad , \quad b_R = -\frac{1}{2} N_\chi''(\chi_C) \tag{4.77}$$

To solve the above Riccati equations, we consider the related Airy equation:

$$\frac{d^2u}{dx^2} - xu = 0 \tag{4.78}$$

Focusing first on the dynamics near A, let us note that the Riccati equation in y_L is satisfied by:

$$y_L = \frac{1}{u}\frac{du}{dx} \tag{4.79}$$

Equation (4.78) solves in terms of a linear combination of the Airy functions Ai and Bi, the linearly independent solutions of this differential equation. Thus, the corresponding Riccati equation (4.74) in y_L admits as its general solution:

$$y_L(x_L) = \frac{Ai'(x) + C_1 Bi'(x)}{Ai(x) + C_1 Bi(x)} \tag{4.80}$$

The constant C_1 is determined by the asymptotic matching condition:

$$\lim_{x_L \to \infty} y_L(x_L) \sim x^{1/2} \tag{4.81}$$

This fixes $C_1 = 0$. The solution is thus:

$$y_L\left(x_L\right) = \frac{Ai'(x_L)}{Ai(x_L)} \tag{4.82}$$

where $Ai\left(x\right)$ has the integral representation:

$$Ai\left(x\right) =_{df} \frac{1}{\pi}\int_0^\infty \cos\left(\frac{t^3}{3} + xt\right)dt \tag{4.83}$$

The solution to the equation (4.74) in y_L given above has the property that it diverges as x_L approaches the the first negative root α_0 of Ai. The location of this root thus determines the $O(\varepsilon^{2/3})$ correction to the change in X_a as the integral curve sweeps from the left to the right branch of the χ-nullcline.

By symmetry, it follows that

$$y_R\left(x_R\right) = -\frac{Ai'(-x_R)}{Ai(-x_R)} \tag{4.84}$$

solves the Riccati equation for y_R given in (4.74), which describes the system's trajectory in the turning regime near C.

Integration of the transition-layer equation (4.57), (again by separation of variables) gives the durations T_{AB} and T_{CB} of the outer portions of the limit cycle:

$$T_{AB} = \int_{X_{aA}}^{X_{aA}+\varepsilon^{2/3}\alpha_0\psi_{xL}} \frac{1}{\varepsilon\left(\psi_{yL}Ai\left(\frac{X'_a}{\psi_{xL}}\right) - X'_a\right)} dX'_a \tag{4.85}$$

$$T_{CD} = \int_{X_{aC}}^{X_{aC}-\varepsilon^{2/3}\alpha_0\psi_{xR}} \frac{1}{\varepsilon\left(\psi_{yR}Ai\left(-\frac{X'_a}{\psi_{yR}}\right) + X'_a\right)} dX'_a \tag{4.86}$$

where α_0 is the first negative root of the Airy function Ai.

4.2.3 Inner phase $\sim O(\varepsilon)$

During the fast inner phase, the viscous drag coefficient $\mu(\chi)$ plummets, becoming negative, and the effective inertial and viscous forces balance, while the effective elastic force is negligible:

$$F_{inertial} \sim F_{viscous} \quad , \quad F_{elastic} \ll F_{viscous} \tag{4.87}$$

The dissipation coefficient μ becomes negative and large, and the velocity v grows explosively:

$$\frac{dv}{dt} \sim -\mu \; v \tag{4.88}$$

Since the acceleration $\frac{dv}{dt}$ is related to the slope $\frac{dv}{d\chi}$ of the integral curve in the (χ, v) plane by:

$$\frac{dv}{dt} = v\frac{dv}{d\chi} = F_{elastic} - \mu v \tag{4.89}$$

we obtain, upon neglecting $F_{elastic}$ in the above approximate equation:

$$\frac{dv}{d\chi} = -\mu \tag{4.90}$$

Integrating (4.90) with respect to χ gives the velocity v explicitly as a function of χ:

$$v_{upstroke}(\chi) = -\int_{\chi_{init}}^{\chi} \mu(\chi')d\chi' = (1+\varepsilon+\varepsilon\kappa_a)(\chi-\chi_{init})+[p_o(\chi) - p_o(\chi_{init})]+v_{init} \tag{4.91}$$

where the constants are determined by matching at $t \to -\infty$ with the transition layer.

In the (χ, X_a) phase plane the inner portion of the integral curve follows:

$$X_a(\chi) \sim \Psi_\chi(\chi) - \frac{1}{\kappa - \varepsilon\kappa_a}\int^{\chi} \mu(\chi')d\chi' \tag{4.92}$$

Having constructed an asymptotic approximation to the limit cycle of system, we can deduce estimates of both the period and amplitude of the limit cycle as a function of the parameters of the system. The estimates are accurate to $O(\varepsilon^{2/3})$

$$T = T_{AB} + T_{BC} + T_{CD} + T_{DA} \quad , \quad A_\chi = \frac{1}{2}\left(\chi_C - \chi_A\right) \tag{4.93}$$

4.2.4 Electrically-evoked otoacoustic emissions

Sinusoidal electrical stimulation produces three distinct patterns of mechanical response [2] (Figure 4.2). At driving frequencies below the intrinsic frequency of the oscillating bundle, the bundle's movement exhibits bursts of rapid oscillations separated by periods of quiescence. At driving frequencies near the intrinsic frequency of oscillation, the bundle's movement shows a biphasic response. At frequencies above the intrinsic frequency, the bundle's movement is sinusoidal and phase-locked to the stimulus. In experimental studies, phase-locking is lost at very high frequencies; the phase-locked state is destroyed by noise when the response amplitude falls below the amplitude of intrinsic fluctuations in the bundle's dynamics.

The electrically evoked oscillations of the hair bundle can be explained under the hypothesis that the motor nonlinearity parameter is a linear function of the cell's membrane potential V_m:

$$\eta_a = \eta_{a,0} + \alpha V_m \tag{4.94}$$

Simulations incorporating this hypothesis agree qualitatively with experimental data on the response of the hair bundle to sinusoidal electrical

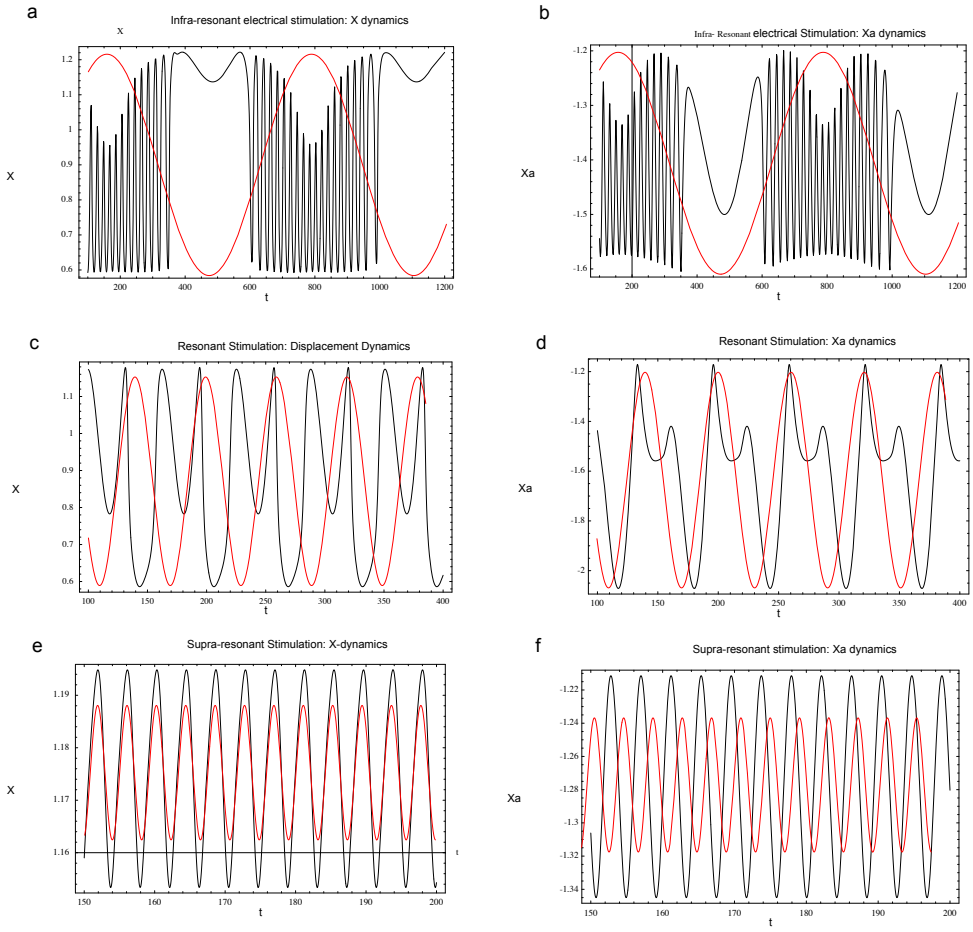

Figure 4.2: *Response of the oscillating hair bundle to sinusoidal electrical stimulation*

a), b) Infra-resonant stimulation; c,d) resonant stimulation; e),f) supra-resonant stimulation. The red curve shows the electrical stimulus V_m, where $\eta_a \equiv \eta_a(V_m) = \eta_{a,0} + \alpha V_m$.

stimulation.

Chapter 5

The hair bundle's response to mechanical stimulation

In this section, we examine the response of the active hair bundle to sinusoidal mechanical stimulation. In particular, we investigate the frequency specificity and nonlinear gain that may underlie mechanical amplification by auditory organs.

5.1 Response to weak forcing

If the hair bundle is initially prepared away from its steady state and

then released; or if, as we consider in this section, it is acted upon by a weak sinusoidal mechanical force, its behavior, to linear order in the state variables, can be studied by Laplace transformation of its dynamical equations. Laplace transformation yields *complex transfer functions* that can be interpreted as the system's gain, giving the ratio of system's output to its input as a function of the frequency with which it is forced. More precisely, if Γ_L denotes the complex transfer function of a system L, the sinusoidal response $A(t)$ of the system to a forcing $F\cos(\omega t)$ of amplitude F and driving frequency ω is given by:

$$A(t) = |\Gamma_L| F\cos[\omega t + \phi(\omega)] \quad , \quad \phi(\omega) = \arctan\left[\frac{Im[\Gamma_L]}{Re[\Gamma_L]}\right] \tag{5.1}$$

We derive by Laplace transformation of equation (2.55), the *complex transfer functions* Γ_{load}, Γ_{fb}, Γ_{amp},and Γ_{Ph}:

$$\Gamma_{load} =_{df} \frac{1}{s^2 + s\mu_\infty + k_\infty} \quad , \quad \Gamma_{fb} =_{df} (s\mu_f + k_f)\frac{d\phi}{d\chi} \quad , \quad \Gamma_{amp} =_{df} \frac{1}{1 + \Gamma_{load}\Gamma_{fb}} \tag{5.2}$$

$$\delta\phi_{fb} = \Gamma_{fb}\delta\chi \quad , \quad \delta\chi = \Gamma_{load}\left(-\delta\phi_{fb} + F\right) \tag{5.3}$$

$$\Gamma_{Ph} = \Gamma_{amp}\Gamma_{load} = \frac{1}{s^2 - sTr_A + Det_A} \tag{5.4}$$

Block diagrams depicting the linear response properties of the passive and active subsystems of the hair bundle are given in Figure 5.1.

The Pade approximation to the simplified model allows for an analytic solution to the complex transfer functions above.

We analyse four properties related to the complex transfer function: 1) the *quality factor* Q; 2) the *maximal gain* $|\Gamma_{max}|$ and 3)frequency at maximal gain (or *best frequency*) ω_b, and the gain-bandwidth product (GBP). For the transfer function Γ_{Ph}, these are defined as:

$$Q_{Ph} =_{df} \frac{\sqrt{k_e}}{\mu} \quad , \quad \omega_{Ph,max} = \sqrt{k_e - \frac{1}{2}\mu^2} \tag{5.5}$$

a. Closed-loop description with input F_{ext}, output χ, and feedback signal ϕ_{fb}

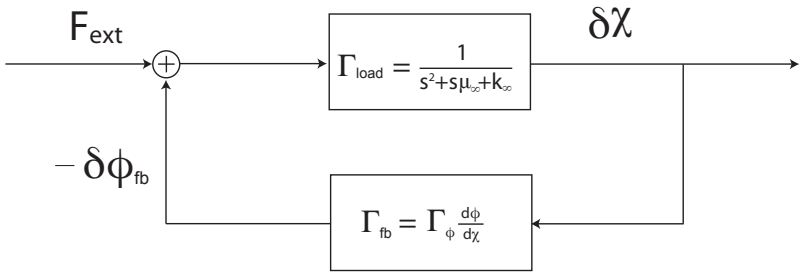

b. Open-loop amplfier-load description with input F_{ext} and output $\delta\chi$

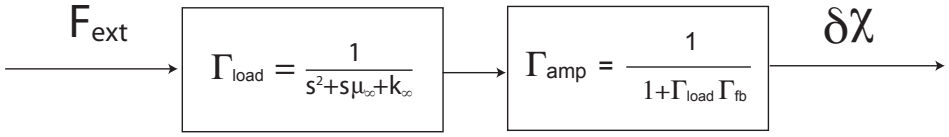

Figure 5.1: *Linear response of the simplified model*
a. Feedback description of the simplified model. b. Equivalent cascade circuit for the linearized feedback system.

$$|\Gamma_{Ph,max}| = \frac{1}{\sqrt{\mu^2\left(k_e - \frac{\mu^2}{4}\right)}} \quad , \quad GBP_{Ph} = \frac{1}{\sqrt{k_e\left(k_e - \frac{\mu^2}{4}\right)}} \tag{5.6}$$

To illustrate the analysis of these linear response properties, consider the problem of characterizing the hair bundle's frequency specificity. The hair bundle may be said to exhibit *frequency specificity* to weak forcing if its stable fixed points have eigenvalues with non-zero imaginary parts. The condition ensuring this (i.e.: the condition that the eigenvalues have an oscillatory component) is:

$$\mu^2 < 4k_e \tag{5.7}$$

or, equivalently,

$$Q_{Ph} > \frac{1}{2} \tag{5.8}$$

Because it gives analytic estimates of μ and k_e, the Pade approximation allows us to demarcate the region of frequency specificity for which condition (5.8) obtains.

Near a Hopf bifurcation, the bundle's response depends nonlinearly upon

the stimulus amplitude. Consider again the van der Pol-Duffing oscillator at the operating point $\chi^* = 0$ and suppose μ_0 small but positive. In this case, for weak forcing (i.e.: for forcing amplitudes $\sim O(\mu_0 \mu_{nl}^{-1})$), the nonlinear response function may be calculated by the Poincare-Lindstedt method, which amounts to the assumption that most of the energy of the forced system's response will be concentrated at the driving frequency rather than at its harmonics. By this method, the complex transfer function is found to be:

$$\Gamma_h = |\Gamma_h| \exp[i\psi_h] \tag{5.9}$$

where

$$|\Gamma_h|^2 = \left|\frac{A}{F}\right|^2 = \frac{1}{\left(\omega_h^2 - \omega^2\right)^2 + \mu_h^2 \omega^2} \quad , \quad \psi_h = \arctan\left[\frac{\mu_h\ \omega}{k_h - \omega^2}\right] \tag{5.10}$$

$$k_h \equiv k_h(A) =_{df} k_0 + \frac{3}{4} k_{nl} A^2 \quad , \quad \mu_h \equiv \mu_h(A) =_{df} \mu_0 + \frac{1}{4} \mu_{nl} A^2 \tag{5.11}$$

As a function of the forcing amplitude and frequency, we define response properties analogous to the linear response properties given above:

$$Q_h = \frac{\sqrt{k_h}}{\mu} \quad , \quad \omega_{max,h} = \sqrt{k_h - \frac{\mu_h^2}{2}} \tag{5.12}$$

$$|\Gamma_{max,h}|^2 = \frac{1}{\mu_h^2\left(k_h - \frac{\mu_h^2}{4}\right)} \quad , \quad GBP_{Ph} = \frac{1}{\sqrt{k_h\left(k_h - \frac{\mu^2}{4}\right)}} \tag{5.13}$$

The relative sensitivity to forcing is given by the equation:

$$\frac{F}{A}\frac{dA}{dF} = 1 + \frac{F}{\Gamma_h}\frac{d\Gamma_h}{dF} \tag{5.14}$$

Thus, the nonlinear response in the weak forcing regime resembles in form the linear response; at fixed forcing amplitude, the response function is of the same form to as a linear response function; the effective stiffness k_h and drag μ_h that enter the response function depend upon the squared amplitude of the response. The Poincare-Lindstedt method provides an approximation to the dependence upon the forcing amplitude.

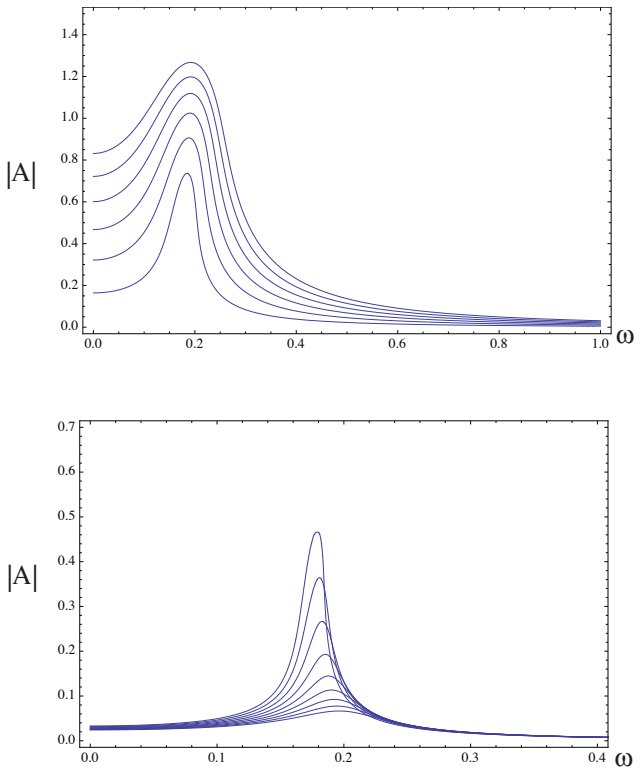

Figure 5.2: *Nonlinear response to weak forcing*
a. Response amplitude as a function of frequency in the parameter regime: ($\varepsilon = 0.11$, $\eta = 4.9$, $\eta_a = 0$, $\kappa = 0.5$, $\kappa_a = 1$, $C = -2.45$). As F_{ext} is increased from 0.005 to 0.03, the gain and quality factor of the response decreases. b. Response amplitude at fixed forcing amplitude for various values of ε in the parameter regime: ($F_{ext} = 10^{-3}$, $\eta = 4.9$, $\eta_a = 0$, $\kappa = 0.5$, $\kappa_a = 1$, $C = -2.45$). As ε is lowered from 0.15 to 0.11, the peak response at constant forcing amplitude increases, and the natural frequency diminishes

5.2 Full nonlinear response

For strong stimuli, the Taylor approximation above leads to inaccurate results, since it fails to capture adequately saturation of the hair bundle's active response. However, we can apply the Poincare-Lindstedt method directly to the Pade-approximated model; analysis of the resulting amplitude-forcing relations for strong reduces to solving cubic and quadratic equations. As shown in Figure 5.3, the approximate nonlinear response function agrees well with the nonlinear response calculated by numerical simulation.

How does the active process affect the compressive nonlinearity seen in the hair bundle's response to sinusoidal mechanical stimulation? To examine this issue, we consider the dynamics of the system under the *locked-motor condition* in which all motion of the X_a variable is abolished. The force-balance relation for this regime involves viscous, elastic, and external forces:

$$0 = F_{viscous} + F_{elastic} + F_{ext} \tag{5.15}$$

where

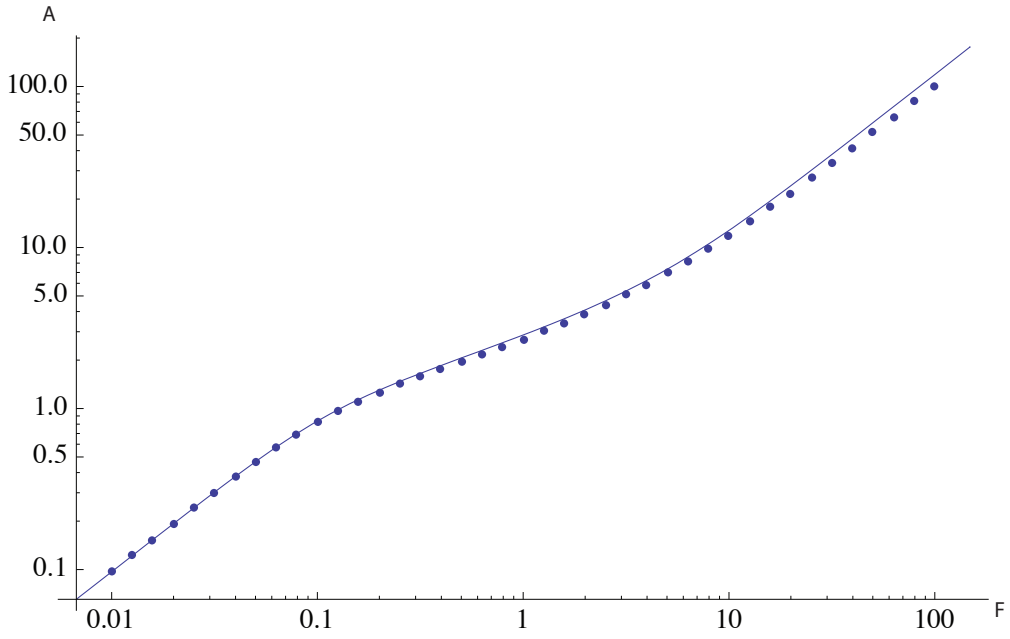

Figure 5.3: *Nonlinear response to weak and strong forcing*
The points indicate values computed by numerical integration of the dynamical equations. The solid line indicates the nonlinear response function calculate by the Poincare Lindstedt method from the Pade-approximated model.

$$F_{viscous} = -\frac{d\chi}{dt} \quad , \quad F_{elastic} = -\chi + \eta p_o + (C - X_{a,locked}) \quad , \quad F_{ext} = G_1 cos[\omega t] + G_2 \sin[\omega t] \tag{5.16}$$

Both simulation and analytic calculations show that tthe nonlinear gating compliance term $\eta\ p_o$ is sufficient to produce a prominent compressive nonlinearity, even in the absence of an active process.

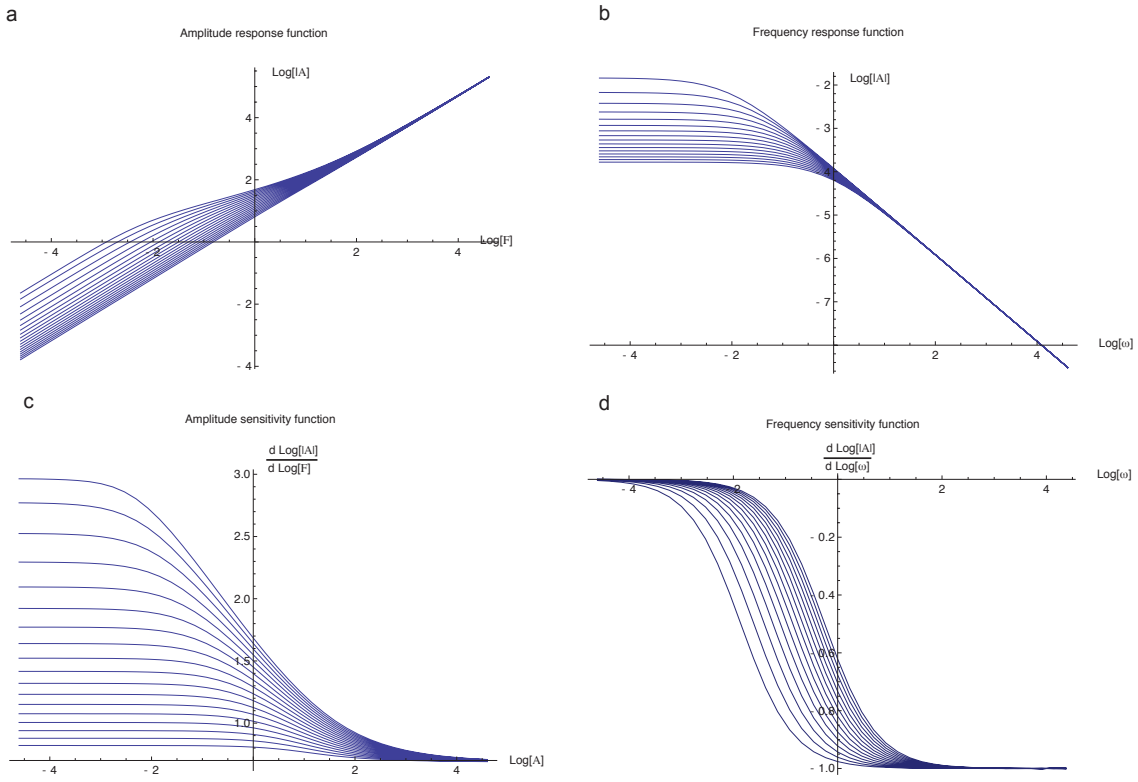

Figure 5.4: *Nonlinear response compression of the hair bundle's dynamics in the locked-motor regime.*

Log response (a, b) and sensitivity (c,d) as a function of logarithm of the stimulus amplitude F_{ext} and stimulus frequency ω. The motor-locked model, with parameter C_{locked} chosen so that the $p_o(\chi_{s.s.}) = 1/2$. As the parameter η sweeps between 0.5 and 3.9, the system's response becomes increasingly nonlinear. a) The amplitude response curves (a,c) show, at fixed frequency ($\omega = 0.1$), the response and sensitivity of the system as a function of stimulus amplitude, for varying values of the non-linearity parameter η and the operating point $p_o(\chi)$. The frequency response curves show, at fixed stimulus amplitude ($F_{ext} = 0.01$), calculate the response and sensitivity of the system as a function of stimulus frequency, for varying values of the non-linearity parameter η and the operating point $p_o(\chi)$.

Chapter 6

Control of the hair bundle's tuning

6.1 Tuning to a Hopf bifurcation through regulation of the motor drag

In the previous section, we explored the biophysical mechanisms underlying the hair bundle's response to sinusoidal mechanical stimulation. We characterized how the gain, natural frequency, and quality factor varies with the system's proximity to a Hopf bifurcation. In this section, we consider the hypothesis that the hair bundle's proximity to the Hopf bifurcation is regulated *in vivo* by adjustment of the drag coefficient λ_a of the hair bundle's adaptation motor.

The drag coefficient λ_a enters into a single dimensionless parameter of the model, namely the time-scale parameter ε, with which it varies inversely:

$$\lambda_a \sim \frac{1}{\varepsilon} \tag{6.1}$$

In view of this relation, we study the problem of tuning ε in the simplified model. Figure 6.1 shows the dependence of the quality factor (at best linear frequency) and the maximal gain (at best linear frequency) ofnthe forcing amplitude and the parameter ε.

Below, we discuss four observations supporting the hypothesis that regulation of λ adjusts the tuning of the hair bundle *in vivo*.

1. The operating point is independent of ε.

The motor drag parameter λ_a is the only biophysical parameter entering into the simplified model to leave the location of the system's fixed points unperturbed; all other biophysical parameters enter as factors into the dimensionless structural parameters (namely η, η_a, κ, κ_a, and C) that set the operating point. That the fixed points are independent of ε follows at once by inspection of the fixed-point equation (3.1), from whose right-hand side ε may be removed by division.

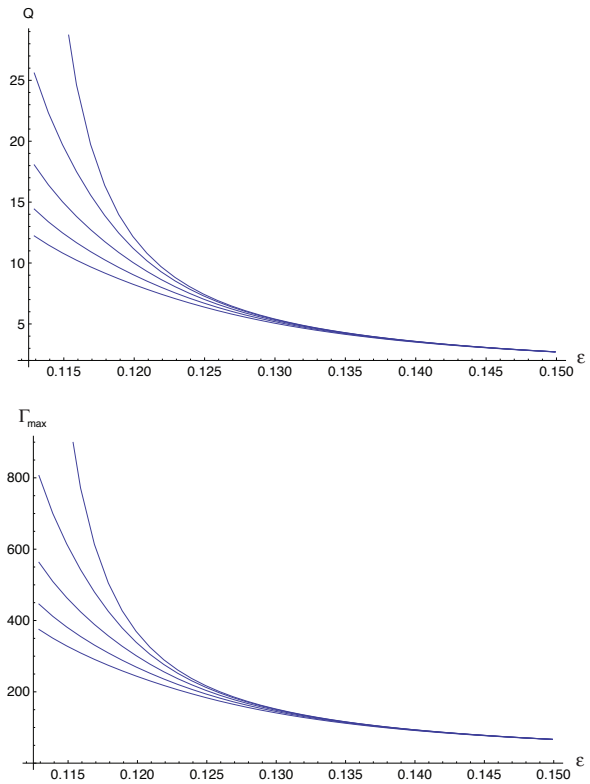

Figure 6.1: *Nonlinear response to weak forcing as a function of the time-scale parameter* ε

a. Quality factor at best linear frequency as the stimulus amplitude F is varied from 1 10^{-3} to 1.5 10^{-3}. At fixed ε, the quality factor diminishes for increasing F. b. Maximal gain at best linear frequency. At fixed ε, the maximal gain diminishes for increasing F. Parameter regime: ($\eta = 4.9$, $\eta_a = 0$, $\kappa = 0.5$, $\kappa_a = 1$, $C = -2.45$)

2. The stability of the cubic term in the amplitude equation near the Hopf bifurcation depends only weakly on ε

For the case of a bundle whose operating point is at $\chi^* = 0$, the sign σ_ε of the cubic term in the amplitude equation for χ, is given by:

$$\sigma_\varepsilon =_{df} sign\left[(\eta - \varepsilon\eta_a)\,\frac{d^2 p_o}{d\chi^2}\right] \tag{6.2}$$

If σ_ε is positive, the cubic term in the amplitude equation will be stabilizing.

So long as the critical value $\varepsilon_{slipping}$ at which the drag coefficient vanishes is far from ε_{sub} at which σ_ε changes sign, tuning to the Hopf bifurcation will leave unchanged the *direction* of the Hopf bifurcation (that is, will not change whether the bifurcation is supercritical or subcritical):

$$\varepsilon_{sub} = \frac{\eta}{\eta_a} \quad , \quad \varepsilon_{slipping} = \frac{\eta - \alpha_{\varepsilon,slipping}}{\eta_a} \tag{6.3}$$

3. Under weak restrictions on the form of the feedback, slow feedback

of the system's activity upon the parameter ε tunes the simplified model robustly to the Hopf bifurcation.

A feedback mechanism in ε, insofar as it involves the activity of the hair bundle's variables (e.g.: χ or ϕ), need depend only minimally, if at all, upon the bundle's structural parameters. Thus, the same tuning mechanism could be used by hair cells ranging widely in the values of their structural parameters.

Moreover, simulations show that feedback schemes in ε tune the bundle to the Hopf bifurcation even under circumstances in which the assumptions of the simplified model fail. For instance, If inertial effects are signifiant, tuning in ε nevertheless succeeds in bringing to the system to a Hopf bifurcation.

4. In vitro *data are consistent with the hypothesis that the motor-drag parameter constitutes the hair bundle's control parameter.*

Pharmacologic experiments on oscillating hair bundles suggest that as the phosphorylation state of the myosin motor is raised the frequency of oscillation diminishes and the amplitude of oscillation is increased [14]. Simulations and analysis shows that these effects can be explained by the hypothesis that phosphorylation of the adaptation motor increases the drag parameter λ_a.

On the basis of these observations, we propose that hair cell regulates biochemically the parameter λ_a to adjust the bundle's proximity to the Hopf bifurcation.

Chapter 7

Discussion

Tuning in the organs of the inner ear arises from three kinds of mechanism: i) mechanical and electrical processes internal to the hair cell; ii) static or slowly-varying mechanisms of supporting mechanical systems that constrain the motion of the hair-cell soma and the hair bundle; and iii) neural mechanisms that relay signals to the brain, and that provide feedback from the brain to the periphery.

Coupling between active hair-bundle motility and the electro-mechanical processes of the hair-cell soma is likely to influence the tuning of some hair cells. In outer hair cells of the cochlea, for instance, the interaction between the active hair bundle and the prestin-mediated electromotile mechanism is likely to underlie mechanical amplification by of acoustic signals. The electrical resonance observed in the hair cells of some reptiles and amphibians filters the mechano-electrical signal transduced by the hair bundle, and may also influence the bundle's mechanics [10, 9, 12, 6].

Static features of the inner ear contribute to tuning by helping to focus the flow of stimulus energy upon the sensory epithelium. Both the hydrodynamic properties of the fluid that fills the bony chambers of the inner ear, and the geometry of the chambers themselves, shape the mechanical responses of the ear's sensory epithelia. The geometry of mammalian semi-circular canals, for instance, appears to be near optimal, given the mechanical constraints on the materials of the organ [19]. Similarly, the spiral geometry of the cochlea may enhance mechanical amplification in this organ by favoring the concentration of cochlear travelling-wave energy toward the outer cochlear wall [13] .

The tissues and acellular structures of that support hair cells play a prominent role in tuning the inner-ear organs. In the cochlea, hair cells rest upon Deiter cells and proteinaceous matter that constitutes the basilar membrane. Mechanical stimulation by the middle ear engenders a the travelling-wave upon the cochlear partition whose dynamics are set by the mechanics of the fluid and the tissue of the basilar membrane. Longitudinal variation in the stiffness of the basilar membrane is among the principal determinants of tuning in the cochlea. [21].

The acellular structures that overlie the hair bundle, such as the tectorial membrane in the cochlea and the otolithic membrane in the sacculus, alter the mechanics of the hair bundle, by imposing upon it an inertial load and possibly a static tensile force.

Finally, the afferent fibers that contact the hair cells themselves are tuned; in the cochlea, afferent fibers vary in their thresholds and dynamic range. Efferent innervation modulates the electrical activity of both afferent fibers and hair cells.

The analysis presented in this paper has a number of limitations. First, it neglects interactions between the hair bundle and the tuning mechanisms just described, namely those of the hair-cell soma, the supporting mechanical structures, and the neural mechanisms of the inner ear. Second, the adiabatic-elimination assumption at the heart of the procedure leading to the simplified model is invalid for hair bundles responding to signals of frequencies greater than $\sim$1kHz, a mid-range frequency for many auditory organs. As the stimulus period approaches the time-scale for the opening and closing of the mechano-sensitive channels, the channel population can no longer be approximated as being in thermodynamic equilibrium, and hence the open probability p_o enters as an additional degree of freedom. It is both an experimental and theoretical open problem to characterize the hair bundle's response to high-frequency signals.

Two additional features of inner-ear organs complicate the tuning problem. First, many auditory organs and possibly other inner-ear organs have distinct sub-populations of hair cells specialized either for the transduction of sound or for its amplification [4]. This division of labor is likely to be associated with differences in tuning mechanism. Second, the coding scheme

employed by the inner-ear organs depends upon the activity of the entire population of hair cells. This means that the effectiveness of an individual hair cell's tuning depends upon the tuning of the other hair cells in the organ.

These considerations lead to a fundamental problem about the tuning of the inner ear: How could local feedback mechanisms, such as those of the active process, tune hair cells effectively, when the condition for optimal tuning of each hair cell is both causally (i.e.: through mechanical coupling of hair cells) and functionally (i.e.: through the population coding scheme) contingent upon the tuning properties of the entire population of hair cells in the organ? Are global mechanisms, such as neurally-mediated coupling through efferent feedback, essential for effective tuning in the inner ear, or could such tuning occur purely through self-organization of the sensory epithelium?

Appendix A

Model Formulation

In section (A.1) of this supplement to "Tuning of the Active Hair Bundle," we present a detailed model of the saccular hair bundle and simplify this model to arrive at a pair of nonlinear dynamical equations in the gating extension χ and the position X_a of the adaptation motor. In section (A.2), we describe how to estimate from data the parameters of the simplified model. In section (A.3), we discuss the accuracy of the Pade approximation to the simplified model. In section (B.1), we apply the method of normal forms to calculate the dynamics of the hair bundle in the near-bifurcation regime. In section (**??**), explore the dynamics of the saccular hair bundle in the excitable regime.

A.1 Model formulation

A.1.1 Detailed model

Force-balance equation for the hair bundle:

$$m_{HB}\frac{d^2x}{dt^2} + \lambda_{HB}\frac{dx}{dt} + \kappa_{SP}(x - x_{SP}) + N_{GS}\gamma\,\kappa_{GS}(\gamma x - x_a + x_c - p_o d) = F_{Ext} \tag{A.1}$$

Kinetic equation for gating of the transduction channel:

$$\frac{dp_o}{dt} = k_{C\to O}(1 - p_o) - k_{O\to C}p_o \tag{A.2}$$

Force-balance equation for the adaptation complex:

$$\lambda_a\,\frac{dx_a}{dt} + p_b N_m f_m - N_{GS}\kappa_{GS}(\gamma x - x_a + x_c - p_o d) + \kappa_{ES}x_a + F_{\lim} = 0 \tag{A.3}$$

Kinetic equations for interaction of the adaptation motor with Ca^{2+} and with actin.

$$\frac{dp_{b,0}}{dt} = k_{m,41}\,p_{b,Ca} + k_{m,21}\,p_{u,0} - (\,k_{m,14}\,c + k_{m,12})\,p_{b,0} \tag{A.4}$$

$$\frac{dp_{u,0}}{dt} = k_{m,12}\, p_{b,0} + k_{m,32}\, p_{u,Ca} - (\, k_{m,23}\, c + k_{m,21})\, p_{u,0} \tag{A.5}$$

$$\frac{dp_{b,Ca}}{dt} = k_{m,14}\, c\, p_{b,0} + k_{m,34}\, p_{u,Ca} - (\, k_{m,41} + k_{m,43})\, p_{b,Ca} \tag{A.6}$$

Current-balance equation for the hair cell:

$$C_m \frac{dV_m}{dt} = -N_{GS} g_{HB} p_o (V_m - E_{HB}) - g_{baso}(V_m - E_{baso}) \tag{A.7}$$

Kinetic coefficient for the open-to-closed transition of the transduction channel:

$$k_{O\to C} \equiv k_{O\to C}(x, x_a) =_{df} \kappa_{trans} \exp\left[-\frac{\Delta E^{\emptyset}_{C\to B} + \delta\, \kappa_{GS}\, \gamma d\, \left(x - \frac{x_a}{\gamma}\right)}{k_B\, T} \right] \tag{A.8}$$

Kinetic coefficient for the closed-to open transition of the transduction channel:

$$k_{C\to O} \equiv k_{C\to O}(x, x_a) =_{df} \kappa_{trans} \exp\left[-\frac{\Delta E^{\emptyset}_{O\to B} + (1-\delta)\, \kappa_{GS}\, \gamma d\, \left(x - \frac{x_a}{\gamma}\right)}{k_B\, T} \right] \tag{A.9}$$

Limiting force on the motor:

$$F_{lim} = U_a exp\left(Z_a(l_a - x_a)\right) \tag{A.10}$$

Stereociliary mechanics

Equation (A.1) describes the balance of forces acting upon the hair bundle [14]. Mechanically, the hair bundle behaves as a damped, cantilevered beam with non-linear elastic properties. m_{HB} denotes the mass of the bundle and λ_{HB} its drag coefficient. The stereociliary pivots have a combined stiffness κ_{SP}; x_{SP} denotes the rest position assumed by the bundle upon severing its gating springs; N_{GS} is the number of gating springs, each of which has a stiffness κ_{GS}. The geometric gain factor γ relates displacements along the bundles axis of excitability to displacements in the direction of movement of the adaptation motor [**?**]; thus, the displacement x of the bundle along its axis of excitability corresponds to a displacement γx in the direction of stretch of the gating springs and of motion of the adaptation complex. The gating length d is the distance by which a gating spring shortens upon the opening of its associated transduction channel [5].

The mean slackening of the gating springs due to opening of the transduction channels is thus $-p_o d$, and the extension of the hair bundles gating

springs is given by $(\gamma x - x_a - p_o d)$. By virtue of their mechanically parallel configuration, the gating springs of the hair bundle exert upon it a combined force $N_{GS}\gamma(\gamma x - x_a - p_o d)$.

An experimental probe or a sensory stimulus subjects the bundle to an external force F_{ext}. Balancing against F_{ext} are the inertial force of the bundle $m_{HB}\frac{d^2x}{dt^2}$; the hydrodynamic drag force $\lambda_{HB}\frac{dx}{dt}$ that resists its motion; and two elastic forces acting in parallel: i) the linear restoring force $\kappa_{SP}(x - x_{SP})$ due to the elasticity of the stereociliary pivots; and ii) the non-linear force $N_{GS}\gamma(\gamma x - x_a - p_o d)$ contributed by the parallel array of gating springs that couple to the bundles mechanosensitive transduction channels [14].

Transduction-channel kinetics

Equation (A.2) describes the kinetics of the open probability of the transduction channels. The kinetic coefficients $k_{O\to C}$ and $k_{C\to O}$, as described by equations (A.8) and (A.9), are postulated to be Arrhenius relations [5, **?**], whose form is:

$$k_{a\to b} = \kappa_{trans} \exp\left(\frac{\Delta E_{a\to b}}{k_B T}\right) \tag{A.11}$$

where $\Delta G_{a\to b}$ is the energy change associated with surmounting the energy barrier separating a from b.

We assume that the transduction channel has two states, open and closed, separated by a transition state at which the channel gate, whose swing has length d, is open by the amount δd, where δ lies between 0 and 1[5]. We denote the energies associated with these states as $E_O^{\emptyset}$, $E_C^{\emptyset}$, and $E_B^{\emptyset}$, respectively, and assume them to vary quadratically in the stretch of the gating spring. Accordingly, the energy differences vary linearly:

$$\Delta E_{C\to B} =_{df} \delta\,\kappa_{GS}\gamma\,d\left(x-\frac{x_a}{\gamma}\right)+\Delta E^{\emptyset}_{C\to B} \tag{A.12}$$

$$\Delta E^{\emptyset}_{C\to B} = \left(E_B^{\emptyset}-E_C^{\emptyset}\right) \tag{A.13}$$

$$\Delta E_{O\to B} =_{df} (1-\delta)\,\kappa_{GS}\gamma\,d\left(x-\frac{x_a}{\gamma}\right)+\Delta E^{\emptyset}_{O\to B} \tag{A.14}$$

$$\Delta E^{\emptyset}_{O\to B} = \left(E_B^{\emptyset}-E_O^{\emptyset}\right) \tag{A.15}$$

$$\Delta E_{C\to O} = \Delta E_{GS}+E^{\emptyset}_{C\to O} \tag{A.16}$$

The total energy difference $\Delta E_{O\to C}$ between the open and closed states is thus the sum of the intrinsic energy difference $E^{\emptyset}_{C\to O}$ with the gating energy difference ΔE_{GS}.

$$\Delta E^{\emptyset}_{C\to O} =_{df} \left(E_O^{\emptyset}-E_C^{\emptyset}\right) \tag{A.17}$$

$$\Delta E_{GS} =_{df} \kappa_{GS}\,\gamma d\,(x - \frac{x_a}{\gamma}) \tag{A.18}$$

Extension of the gating spring changes linearly the relative energy difference between the metastable states of the transduction channel.

Mechanics of the adaptation motor

The motion of the adaptation complex is governed by the balance of forces described in equation (A.3). We adopt the convention [14] that downward displacements of the adaptation complex correspond to positive changes in x_a. The viscous force $\lambda_a \frac{dX_a}{dt}$ upon the adaptation complex, whose drag coefficient we denote by λ_a, is balanced against both elastic forces and an active climbing force exerted by the adaptation motor. Three elastic forces act upon the adaptation motor: *i*) a restoring force $\kappa_{ES} x_a$ due to an extent spring of stiffness κ_{ES} that lies in parallel with the gating spring array; *ii*) the non-linear elastic force $N_{GS}(\gamma x - x_a - p_o d)$ due to the gating-spring array; and *iii*) the term $U_a exp(Z_a(l_a - x_a))$ corresponding to the force felt by the adaptation motor from a limiting element at the upper boundary of the hair bundle that strongly impedes its ascent above the height l_b. In addition to these passive forces, the energy-consuming myosin-based adaptation motor exerts a force $p_b N_m \gamma f_m$. This climbing force is the product of three factors: i) the force per motor f_m; ii) the number of adaptation motors N_m; iii) and the fraction p_b of motors bound to the actin cores of the stereocilia.

Electro-physiology of the hair cell

Equation (A.7) describes the balance of currents for the hair cell[2]. The total current spent in capacitative charging of the membrane must match the currents flowing into the cell across conductive paths through membrane. Four currents flow into the cell: i) the transduction current $I_{HB} = \alpha p_o(V - E_{HB})$; ii) current through the voltage-dependent Ca^{2+} channels at the hair-cell synapses; iii) synaptic current through Ca^{2+}-dependent K^+ channels; and iv) the hair cells leak current. For simplicity, we model the basal currents ii)-iv) collectively as a simple voltage-dependent current.

The concentration c of Ca^{2+} in the vicinity of the adaptation motor affects both the climbing force exerted by the motors upon the adaptation complex and the drag associated with the adaptation complex. This concentration is determined by the instantaneous Ca^{2+} current I_{Ca} whose magnitude is approximately linear in the product of the open probability p_o, and the voltage V_m.

To derive this dependence of c upon p_o and V_m, we consider the effects of three mechanisms that determine the Ca^{2+} dynamics in the hair bundle [**?**]: 1) influx into the cell; 2) diffusion away from the transduction complex; and 3) buffering of Ca^{2+} in the vicinity of the complex.

On the assumption that 1) the current flowing through the channel

rapidly reaches steady state; and that 2) buffering does not substantially influence c, so that a force-flux relation determines the local Ca^{2+} concentration [**?**], the time constant for the decay in the Ca^{2+} concentration due to diffusion in the vicinity of the motor is approximately:

$$\tau_{c,diff} \approx \frac{r_m^2}{D_{Ca}} = \frac{\left(50.10^{-9}\, m\right)^2}{6.10^{-10} m^2 s^{-1}} \approx 10^{-6} s^{-1} \tag{A.19}$$

The time-scale for decay of the Ca^2+ concentration is thus $\tau_{c,diff} \approx 1\mu s$. This time-scale is fast relative to that of signals detected by the sacculus, indeed even relative to the time-scales of high-frequency acoustic stimuli.

The likelihood for a Ca^{2+} ion to bind to a buffer molecule before first diffusing away from the adaptation complex depends upon the concentration c of Ca^{2+}, and the amount of buffer near the transduction channel. The mean time-to-capture of a Ca^{2+} ion by buffer is such that the root mean-square distance that the molecule moves is greater than the linear extent of the adaptation complex. The mean-time-to-capture of Ca^{2+} by buffer is given by:

$$\tau_{buffer} =_d f \frac{1}{k_{on,buffer}[B]} \tag{A.20}$$

where $k_{on,buffer}$ is the rate constant for binding of Ca^{2+} to buffer, and $[B]$ is the concentration of Ca^{2+} buffer in the hair bundle. The root-mean-squared distance that Ca^{2+} diffuses over the duration τ_{buffer} is:

$$y_{rms} \sim \sqrt{D_{Ca}\,\tau_{buffer}} \;=\; \sqrt{(6\,.10^{-10} m^2 s^{-1})\,(10^{-6}\,s)} \sim 20\,nm \qquad \text{(A.21)}$$

It follows that it is highly probable for a Ca^{2+} ion in the vicinity of the adaptation complex to diffuse away from the complex before it encounters a buffer molecule. Accordingly, the effect of buffer upon c may be neglected, and integration of the diffusion equation yields c [**?**], on the assumption that Ca^{2+} diffuses into a hemisphere centered about the channel pore:

$$c = -\frac{1}{D_{Ca}} \int J\, \frac{1}{\frac{1}{2}\,(4\,\pi\,r^2)} dr \qquad \text{(A.22)}$$

J is the Ca^{2+} flux and r_m is the radial distance from the pore of the transduction channel that represents the linear extent of the adaptation complex. The assumption here is that the Ca^{2+} flux changes slowly relative to the time-scale for diffusion away from the adaptation complex. The

relation between the flux J and the Ca^{2+} current into the hair cell is:

$$J = -\frac{I_{Ca}}{z_{Ca}\, F} \tag{A.23}$$

This implies that:

$$c = -\frac{I_{Ca}}{2\,\pi\, z_{Ca}\, F\, D_{Ca}\, r} \tag{A.24}$$

We assume that the Ca^{2+} current I_{Ca} satisfies the Goldman-Hodgkin-Katz equation [14]. P_{Ca} is the permeability of the channel times the area across which flux into the bundle occurs, e is the unit electrical charge, z_{Ca} is the valence of Ca^{2+}, and D_{Ca} is the diffusion coefficient of Ca^{2+} in water. Thus, at low membrane potentials, we see that I_{Ca}, and hence c, is proportional to both the external Ca^{2+} concentration, and the open probability p_o. If $V_m \ll \frac{k_B T}{e z_{Ca}}$, then c is also approximately linear in the electrical potential V_m:

$$c = \alpha \left[Ca^{2+}\right]_{ext} p_o \left(V_m - E_{Ca}\right) \tag{A.25}$$

$$\alpha =_{df} \frac{P_{Ca}}{2\pi D_{Ca} r_m} \frac{1}{(k_B T / e z_{Ca})} \tag{A.26}$$

Equations (A.4)-(A.6) describe the kinetics of the adaptation motors interactions with Ca^{2+} and with the actin cores of the stereocilia. These equations assume that the myosin motors are in one of four possible states: 1) dissociated from the actin core but unbound to Ca^{2+} ($M_{b,0}$); 2) associated with the actin core and unbound to Ca^{2+} ($M_{b,Ca}$); 3) associated with the actin core and bound to Ca^{2+} ($M_{b,Ca}$); 4) dissociated from the actin core and bound to Ca^{2+} ($M_{u,Ca}$). The fractions of motors in each of these states are, respectively: $p_{u,0}$, $p_{b,0}$, $p_{b,Ca}$, and $p_{u,Ca}$.

Let N_m represent the total number of myosin motors in the hair bundle. We assume N_m to be constant, so that a conservation relation obtains among the dynamical variables describing the fraction p_b of motors in each of the four possible states:

$$p_{u,c} = 1 - (p_{u,0} + p_{b,0} + p_{b,Ca}) \tag{A.27}$$

A.1.2 Simplified model

In this section, we address the problem of simplifying the detailed model presented above, in order to facilitate both comparison with experiment ad mathematical analysis. To this end, we make use of two procedures: 1) adiabatic elimination of the fast variables of the system; and 2) scaling of the

dynamical equations. Adiabatic elimination reduces the number of dynamical equations and eliminates four parameters, namely the time-scales of the fast variables. Scaling further reduces the number of parameters by grouping them into combinations that consistently recur throughout the analysis of the dynamical equations.

Adiabatic Elimination

Adiabatic elimination is a perturbative approach that involves distinguishing rapidly-evolving from slowly evolving variables, and then assuming that on slow time-scales, the dynamics of the rapidly-evolving variables are always approximately at steady-state. By this assumption, the dynamical equations for the rapidly-evolving variables may be replaced with equations that describe their dependence at steady-state upon the slow variables. In the model of the hair bundle presented above, we adiabiatically eliminate four of the seven dynamical variables, namely p_o, $p_{u,0}$, $p_{b,0}$, and $p_{b,Ca}$. This leaves us with a dynamical system involving three variables: x, x_a, and V_m.

Transitions between the open and closed configurations of the channel occur rapidly relative to the time-scales of motion of the bundle and of its adaptation motor. On these slower time-scales, the transduction channels are approximately in thermodynamic equilibrium, varying quasi-statically with x and x_a.

If the inertial force of the bundle is small compared to the viscous and

elastic forces acting upon the bundle, we can approximate the force-balance equation with a first-order differential equation.

At steady state, p_o satisfies the Boltzmann relation:

$$p_o \equiv p_o(x, x_a) = \frac{1}{1 + \exp[\frac{E_0 - \kappa_{GS}\,\gamma\,d\,(\gamma\,x - x_a + x_c - \frac{d}{2})}{k_B\,T}]} \tag{A.28}$$

At steady-state, with Ca^{2+} concentration c, the fraction p_b of motors bound to the stereocilia is:

$$p_b = \frac{1 + \frac{k_{14}}{k_{43}}c}{1 + (\frac{k_{14}}{k_{21}} + \frac{k_{14}}{k_{32}} + \frac{k_{14}}{k_{43}})c} \tag{A.29}$$

To simplify still further, we suppose that:

$$c \ll \frac{k_{43}}{k_{14}} \quad and \quad c \ll \frac{1}{(\frac{k_{14}}{k_{21}} + \frac{k_{14}}{k_{32}})} \tag{A.30}$$

This implies that

$$p_b \approx \frac{1}{1+(\frac{k_{14}}{k_{21}}+\frac{k_{14}}{k_{32}})c} = 1 - \frac{(\frac{k_{14}}{k_{21}}+\frac{k_{14}}{k_{32}})c}{1+(\frac{k_{14}}{k_{21}}+\frac{k_{14}}{k_{32}})c} \tag{A.31}$$

Thus, at low values of c, p_b will be linear in c:

$$p_b \approx 1 - \left(\frac{k_{14}}{k_{21}}+\frac{k_{14}}{k_{32}}\right)c \tag{A.32}$$

Substituting

$$c = \alpha \left[Ca^{2+}\right]_{ext} p_o \left(V_m - E_{HB}\right) \tag{A.33}$$

gives

$$p_b = 1 - Sp_o \tag{A.34}$$

where S, the *motor sensitivity*, is defined as:

$$S =_{df} (\frac{k_{14}}{k_{21}} + \frac{k_{14}}{k_{32}})\alpha \left[Ca^{2+}\right]_{ext} (V_m - E_{Ca}) \tag{A.35}$$

Under these approximations, we can express force-balance equation for the motor as:

$$(\lambda_a + (1 - S p_o)\lambda_m)\frac{dx_a}{dt} + (1 - S\, p_o)N_m f_{\mathrm{m}} - N_{GS}\kappa_{GS}(\gamma x - x_a + x_c - p_o d) + \kappa_{ES}\,(x_a - x_{ES}) + F_l = 0 \tag{A.36}$$

To put the model in a form amenable to perturbation analysis, we render the dynamical equations dimensionless. We choose scales such that the nonlinear open probability p_o is a function of the scaled extension χ of the gating spring, and has no explicit parameter dependence. This corresponds to choosing an offset constant for χ such that p_o is centered about zero; and choosing a length scale for χ such that the standard deviation of probability-density function $\frac{dp_o}{d\chi}$ is $\frac{\pi}{\sqrt{3}}$.

Dynamical equation for the scaled extension χ of the gating spring:

$$\frac{d\chi}{dt_s} = G_{HB}\left(\chi, X_{a,s}\right) - \varepsilon G_a\left(\chi, X_{a,s}, V_{m,s}\right) \tag{A.37}$$

Dynamical equation for the scaled position X_a of the adaptation motor:

$$\frac{dX_{a,s}}{dt_s} = \varepsilon_a G_a\left(\chi, X_{a,s}, V_{m,s}\right) \tag{A.38}$$

Dynamical equation for the scaled membrane potential V_m:

$$\frac{dV_{m,s}}{dt_s} = -\varepsilon_V G_V\left(\chi, V_{m,s}\right) \tag{A.39}$$

State-function for χ:

$$G_{HB}\left(\chi, X_{a,s}\right) =_{df} -\chi + \frac{\kappa_{NGS,s}}{\sigma} p\left(\chi\right) - \left(1 - \kappa_{NGS,s}\right) X_{a,s} - C_{HB} + F_{ext,s} \tag{A.40}$$

State-function for X_a:

$$G_a\left(\chi, X_{a,s}, V_{m,s}\right) =_{df} \frac{1}{1 - S\lambda_{m,s} p_o}\left[\chi - \left(1 - Sf_{m,s}\right) p_o - \kappa_{ES,s}\, \sigma X_{a,s} - C_a + F_{l,s}\right] \tag{A.41}$$

State-function for V_m:

$$G_V\left(\chi, V_{m,s}\right) =_{df} g_{HB,s} p_o \left(V_{m,s} - E_{HB,s}\right) + \left(V_{m,s} - 1\right) \tag{A.42}$$

Open probability:

$$p_o \equiv p_o\left(\chi\right) =_{df} \frac{1}{1 + \exp[-\chi]} \tag{A.43}$$

Motor senstivity:

$$S \equiv S\left(V_{m,s}\right) =_{df} S_o + \alpha_S V_m \tag{A.44}$$

Limiting force:

$$F_{l,s} \equiv F_{l,s}\left(X_{a,s}\right) =_{df} U_{a,s} \exp\left[Z_{l,s}\left(l_s - X_{a,s}\right)\right] \tag{A.45}$$

$$V_{m,s} =_{df} \frac{V_m}{E_{baso}} \tag{A.46}$$

$$l_s =_{df} \frac{l}{\psi_{xa}\sigma} \quad , \quad Z_{l,s} =_{df} \frac{Z_l}{\left(\psi_{xa}\sigma\right)^{-1}} \tag{A.47}$$

$$F_{ext,s} =_{df} \frac{F_{ext}}{\sigma\kappa_{\max}\psi_x} \quad , \quad f_{m,s} =_{df} \frac{f_m}{N_{GS}\kappa_{GS}d} \tag{A.48}$$

$$U_{a,s} =_{df} \frac{U_a}{N_{GS}\kappa_{GS}d} \tag{A.49}$$

Scaled motor drag parameters:

$$\lambda_{a0,s} =_{df} \frac{\lambda_{a0}}{\psi_{\lambda a}} \quad , \quad \lambda_{m,s} =_{df} \frac{\lambda_m}{\psi_{\lambda a}} \tag{A.50}$$

A.1.3 Scaled model

Equations

$$\frac{d\chi}{dt_s} = (\kappa - \varepsilon\kappa_a)\left(\Psi_\chi(\chi) - X_{a,s}\right) \tag{A.51}$$

$$\frac{dX_{a,s}}{dt_s} = \varepsilon\kappa_a\left(\Psi_a(\chi) - X_{a,s}\right) \tag{A.52}$$

$$\Psi_\chi(\chi) =_{df} \frac{1}{\kappa - \varepsilon\kappa_a}\left(-(1+\varepsilon)\chi + (\eta - \varepsilon\eta_a)\, p_o(\chi) - C\right) \tag{A.53}$$

$$\Psi_a(\chi) =_{df} \frac{1}{\kappa_a}\left(\chi + \eta_a p_o(\chi)\right) \tag{A.54}$$

$$p_o(\chi) =_{df} \frac{1}{1 + exp(-\chi)} \tag{A.55}$$

$$0 < \varepsilon \quad , \quad 0 < \kappa < 1 \quad , \quad 0 < \kappa_a \quad , \quad 0 < \eta \quad , \quad -\eta < \eta_a, \quad , \quad -\infty < C < \infty \tag{A.56}$$

Variables

$$\chi = X_s - X_{a,s} \tag{A.57}$$

$$t_s = \frac{t}{\psi_t} \quad , \quad X_s = \frac{X}{\psi_X} + \left[\left(\frac{f_{m,s} - E_{0,s}}{\kappa_{a,s}} - E_{0,s} \right) \right] \quad , \quad X_{a,s} = \frac{X_a}{\psi_{X_a}} + \left(\frac{f_{m,s} - E_{0,s}}{\kappa_{a,s}} \right) \tag{A.58}$$

Parameters

$$\varepsilon = \frac{\lambda_{HB,s}}{\lambda_{a,s}} \quad , \quad \eta = \frac{1-\kappa}{\sigma} \quad , \quad \eta_a = S f_{m,s} - \eta \quad , \tag{A.59}$$

$$\kappa = \frac{\kappa_{SP}}{\psi_\kappa} \quad , \quad \kappa_a = \frac{\kappa_{ES}}{\psi_{\kappa a}} \quad , \quad C = \frac{\kappa}{\kappa_a} f_{m,s} + C_p \tag{A.60}$$

Auxiliary Parameters

$$\lambda_{a,s} = \frac{\lambda_a}{\psi_{xa}\psi_t} \quad , \quad \lambda_{HB,s} = \frac{\lambda_{HB}}{\psi_x \psi_t} \quad , \quad \sigma = \frac{k_B T}{\kappa_{GS} d^2} \tag{A.61}$$

$$C_p = \kappa \left(X_{SP,s} - \left(\frac{\kappa \kappa_a}{\kappa + \kappa_a} \right)^{-1} E_{0,s} \right) \tag{A.62}$$

$$E_{0,s} = \frac{E_0}{k_B T} + \frac{\eta}{2} - \frac{x_c}{\psi_{X_a}} \quad , \quad f_{m,s} = \frac{f_m}{\psi_{\kappa a}\psi_{Xa}} \quad , \quad X_{SP,s} = \frac{x_{SP}}{\psi_X} \tag{A.63}$$

Scales

$$\psi_\kappa = N_{GS}\kappa_{GS}\gamma^2 + \kappa_{SP} \quad , \quad \psi_{\kappa a} = N_{GS}\kappa_{GS} \tag{A.64}$$

$$\psi_t = \frac{\lambda_{HB}}{\psi_\kappa} \quad , \quad \psi_x = \frac{k_B T}{\kappa_{GS}\gamma d} \quad , \quad \psi_{xa} = \frac{k_B T}{\kappa_{GS} d} \tag{A.65}$$

Second-order equation

$$\frac{d^2\chi}{dt_s^2} + \mu(\chi)\frac{d\chi}{dt_s} + \omega_\kappa^2\chi - \omega_\kappa^2 d_\kappa p_o(\chi) - \varepsilon\kappa_a C = 0 \tag{A.66}$$

$$\mu(\chi) =_{df} (1 + \varepsilon + \varepsilon\kappa_a) - \alpha_\varepsilon p_o(\chi)\,(1 - p_o(\chi)) \tag{A.67}$$

$$\alpha_\varepsilon =_{df} \eta - \varepsilon\eta_a \quad , \quad \omega_\kappa =_{df} \sqrt{\varepsilon\,(\kappa + \kappa_a)} \quad , \quad d_\kappa =_{df} \frac{\kappa\kappa_a}{\kappa + \kappa_a}\left(\frac{\eta}{\kappa} - \frac{\eta_a}{\kappa_a}\right) \tag{A.68}$$

$$-\frac{\omega_\kappa^2 d_\kappa}{\varepsilon\kappa_a} < \alpha_\varepsilon < d_\kappa(1+\varepsilon) \quad , \quad 0 < \varepsilon \quad , \quad 0 < \kappa_a \quad , \quad \sqrt{\varepsilon\kappa_a} < \omega_\kappa < \sqrt{\varepsilon(1+\kappa_a)} \tag{A.69}$$

A.2 Parameter Estimation

The nullcline functions Ψ_χ and Ψ_a may be inferred from the force-displacement and current-displacement functions measured under displacement clamp:

$$\Psi_\chi\left(X_{clamped} + X^*_{a,ref}\right) = \frac{1}{(\kappa - \varepsilon\kappa_a)} F_0\left(X_{clamped}\right) \tag{A.70}$$

$$\Psi_a\left(X_{clamped} + X^*_{a,ref}\right) = \frac{1}{\kappa_a}\left(X_{clamped} - Log\left(\frac{I_{HB}/I_{\max}}{1 - I_{HB}/I_{\max}}\right)\right) \tag{A.71}$$

where F_0 represents the scaled instantaneous force-displacement function measured under displacement clamp; $X_{clamped}$ denotes the scaled displacement imposed upon the bundle by the displacement clamp; X^*_a denotes the scaled steady-state position of the adaptation motor at rest.

Below, we describe how to estimate the parameters required to scale the simplified model; and some approaches for estimating the time-scale parameter ε.

A.2.1 Estimating the passive parameters

In this section, we consider the estimation of the parameters κ_{GS} , κ_{SP}, d, E_0, N_{GS}, x_c, and x_{SP}. We denote with a hat the experimentally-derived estimators of the these quantities; thus, for instance, $\hat{\kappa}_{SP}$ denotes an estimator of κ_{SP}. Also we use the symbol $=_{est}$ to signify the relation *being an*

estimator of: thus $A =_{est} B$ means A is an estimator of B.

The instantaneous stiffness κ_{bundle} of the hair bundle is given by:

$$\kappa_{bundle} \equiv \kappa_{bundle}(x, x_a^*) =_{df} N_{GS}\kappa_{GS}\gamma^2[(1 - \frac{\kappa_{GS}d^2}{k_BT}p_o(1-p_o)] + \kappa_{SP} \quad \text{(A.72)}$$

The maximum value $\kappa_{bundle,max}$ of the stiffness is:

$$\kappa_{bundle,\max} =_{df} N_{GS}\kappa_{GS}\gamma^2 + \kappa_{SP} \quad \text{(A.73)}$$

We can estimate $N_{GS}\kappa_{GS}\gamma^2$ by measuring the bundle stiffness upon disrupting the tip-links. The difference in stiffness between the intact bundle and the disrupted bundle in the linear regime is $N_{GS}\kappa_{GS}\gamma^2$.

We define the relative bundle stiffness as:

$$\Delta\kappa_{bundle} =_{df} \kappa_{bundle,\max} - \kappa_{bundle} = \frac{N_{GS}\,(\kappa_{GS}\,\gamma\,d)^2}{k_BT}p_o(1-p_o) \quad \text{(A.74)}$$

The open probability p_o is a cumulative distribution function whose derivative is $p_o(1-p_o)$. Thus, scaling $\Delta\kappa_{bundle}$ by $\frac{N_{GS}(\kappa_{GS}\gamma d)^2}{k_BT}$ yields the probability distribution $\Delta\kappa_{bundle,s}$:

$$\Delta\kappa_{bundle,s} =_{df} \frac{\Delta\kappa_{bundle}}{\left(\frac{N_{GS}\,(\kappa_{GS}\,\gamma\,d)^2}{k_BT}\right)} = p_o\,(1-p_o) \tag{A.75}$$

Thus, the empirical normalization factor for $\Delta\kappa_{bundle}$ gives an estimate of the stiffness scale for the system. The $\Delta\kappa_{bundle,s}$ probability distribution has the property that its peak is:

$$\hat{\psi}_{\kappa,peak} = \frac{1}{4}\frac{N_{GS}\,(\kappa_{GS}\,\gamma\,d)^2}{k_BT} \tag{A.76}$$

The distribution $\Delta\kappa_{bundle,s}$ also has the property that, if the displacement is scaled to $\frac{k_BT}{\kappa_{GS}\gamma d}$, its width varies inversely with its peak height. Noting that:

$$\int_{-\infty}^{\infty} \chi^2 \frac{d}{d\chi} \left(\frac{1}{1 + \exp(-\chi)} \right) d\chi = \frac{\pi^2}{3} \tag{A.77}$$

we obtain an exact relation between width and the peak height of $\Delta\kappa_{bundle,s}$:

$$(width) \times (peak) = \frac{\pi}{4\sqrt{3}} \approx 0.45345 \tag{A.78}$$

The geometric gain factor γ has been estimated from electron-microscopic measurements of hair-bundle morphology. The temperature T is set experimentally, and k_B, the Boltzmann constant is a universal constant. N_{GS} is the number of stereocilia.

The instantaneous current-displacement function provides an independent estimate of the probability density function $\Delta\kappa_{bundle,s}$, since:

$$p_o = \frac{I_{HB}}{I_{HB,\max}} \tag{A.79}$$

The relation between the width and peak of the distribution thus yields an independent estimate of the length-scale.

In sum, the estimators for the passive parameters of the hair bundle that can be extracted from the instantaneous force-displacement curves are:

$$\hat{\kappa}_{\max} =_{est} \kappa_{NGS}+\kappa_{SP} \quad , \quad \hat{\psi}_{\kappa,peak} =_{est} \frac{1}{4}\frac{N_{GS}(\kappa_{GS}\gamma d)^2}{k_BT} \quad , \quad \psi_{x,ch} =_{est} \frac{k_BT}{N_{GS}\kappa_{GS}\gamma d} \tag{A.80}$$

$$\hat{\kappa}_{NGS} =_{df} (\hat{\kappa}_{\max} - \hat{\kappa}_{SP}) \quad , \quad \hat{N}_{GS} =_{df} 4\frac{\hat{\psi}_{\kappa,peak}\hat{\psi}^2_{x,ch}}{\hat{\beta}} \tag{A.81}$$

$$\hat{\kappa}_{GS} =_{df} \frac{\hat{\kappa}_{NGS}}{\hat{N}_{GS}\hat{\gamma}^2} \quad , \quad \hat{\psi}_x =_{df} \frac{\hat{\kappa}_{NGS}}{\hat{N}_{GS}\hat{z}} \tag{A.82}$$

A.2.2 Estimating the drag coefficient λ_{HB}

An analysis of the dynamics of the hair bundle yields an estimate of the drag coefficient λ_{HB}.

Suppose we sever the gating springs so that all of the elastic properties of the bundle are due to the stereociliary pivots. The force-balance equation for the stereocilia under this condition reduces to:

$$\frac{dx}{dt} = -\frac{\kappa_{SP}}{\lambda_{HB}}x + \frac{\kappa_{SP}}{\lambda_{HB}}x_{SP} + F_{ext} \tag{A.83}$$

The time-scale estimated from this experiment for relaxation of the bundle to steady-state following a mechanical perturbation is thus:

$$\psi_{t,severed} =_{est} \frac{\lambda_{HB}}{\kappa_{SP}} \tag{A.84}$$

It follows that λ_{HB} may be estimated by:

$$\hat{\lambda}_{HB} =_{df} \frac{\hat{\kappa}_{SP}}{\hat{\psi}_{t,severed}} \tag{A.85}$$

We can thus construct an estimate of ψ_t:

$$\hat{\psi}_t =_{df} \frac{\hat{\lambda}_{HB}}{\hat{\kappa}_{NGS} + \hat{\kappa}_{SP}} \tag{A.86}$$

The preceding analysis has outlined a procedure for obtaining experimentally-derived estimates of all parameters required to scale the dynamical equations. In light of this, we may deal exclusively with scaled quantities in the analysis that follows. Accordingly, we omit the subscript indicating that the quantities are scaled; unless otherwise noted, all quantities are assumed to be scaled as described above.

A.2.3 Estimating the time-scale parameter ε

Suppose we block the channels with amiloride so that $p_o \equiv 0$.

$$\frac{dX}{dt} = G_{HB}\left(X - X_a, X_a\right) \tag{A.87}$$

$$\frac{d\chi}{dt} = G_{HB,blocked} - \varepsilon G_{a,blocked}\left(\chi, X_a\right) \tag{A.88}$$

$$\frac{dX_a}{dt} = \varepsilon G_a\left(\chi, X_a\right) \tag{A.89}$$

where

$$G_{a,blocked}\left(X - X_a, X_a\right) =_{df} \left[\left(X - X_a - \kappa_{ES}\sigma X_a\right) - C_a + F_{\mathrm{l}}\right] \qquad \text{(A.90)}$$

$$G_{HB,blocked}\left(X - X_a, X_a\right) =_{df} -\left(X_s - X_a\right) - \left[\left(1 - \kappa_{NGS}\right) X_a + C_{HB}\right] \quad \text{(A.91)}$$

We now have a linear dynamical system:

$$\frac{d}{dt}\begin{pmatrix} \delta X \\ \delta X_a \end{pmatrix} = \begin{pmatrix} -1 & \kappa_{NGS} \\ \varepsilon & -\varepsilon\left(1 + \kappa_{NGS}\sigma\right) \end{pmatrix}\begin{pmatrix} \delta X \\ \delta X_a \end{pmatrix} \qquad \text{(A.92)}$$

The eigenvalues of the system are:

$$\Lambda_{blocked} = \frac{1}{2}\left[\left(-1 + \varepsilon + \varepsilon\kappa_{NGS}\sigma\right) \pm \sqrt{\left(1 - \varepsilon - \varepsilon\kappa_{ES}\sigma\right)^2 + 4\varepsilon\left(1 + \kappa_{NGS} + \kappa_{ES}\sigma\right)}\right] \qquad \text{(A.93)}$$

If ε is small, then a series expansion in ε about 0 to linear order yields:

$$\Lambda_{blocked} = -1 - \kappa_{NGS}\varepsilon + O\left[\varepsilon^2\right] \tag{A.94}$$

This gives an estimate of ε:

$$\hat{\Lambda}_{blocked} =_{df} \left(\frac{\hat{\psi}_{t,blocked}}{\hat{\psi}_t}\right)^{-1} \tag{A.95}$$

A.2.4 Relations between the observable and internal variables

The phenomenological equation for the the hair bundle's displacement is

$$X = \chi + X_a \tag{A.96}$$

$$\frac{d^2X}{dt^2} + \mu_X \frac{dX}{dt} + \varepsilon W f_{X,elastic} = 0 \tag{A.97}$$

$$\frac{d\chi}{dt} = (\kappa - \varepsilon\kappa_a)(N_\chi(\chi) + \chi - X) \tag{A.98}$$

where

$$\mu_X(\chi) =_{df} 1 + \varepsilon + \varepsilon\kappa_a - \left(\eta + \varepsilon\frac{1+\kappa_a}{1-\kappa}\right) p_o(\chi)(1 - p_o(\chi)) \tag{A.99}$$

$$W(\chi) =_{df} -\left(\frac{1-\kappa}{\kappa}\right)\frac{N_\chi}{d\chi} = 1 - \left(\frac{\eta}{1-\kappa}\right) p_o(\chi)(1 - p_o(\chi)) \tag{A.100}$$

$$f_{X,elastic}(X,\chi) =_{df} (\kappa + \kappa_a)X - [(1+\kappa_a)\eta - (1-\kappa)\eta_a]p_o(\chi) - (1+\kappa_a)C \tag{A.101}$$

Thus, the variable X and u are related to the variable χ and v by the

equations:

$$X(\chi, v) = \chi + \Psi_\chi - \frac{1}{\kappa - \varepsilon\kappa_a} v \tag{A.102}$$

$$u(\chi, v) = \frac{dX}{dt} = v + \varepsilon\kappa_a(\Psi_a - X + \chi) \tag{A.103}$$

For small amplitudes of movement, this coordinate transformation is approximately linear:

$$\begin{pmatrix} \delta X \\ u \end{pmatrix} = M \begin{pmatrix} \delta\chi \\ v \end{pmatrix} \tag{A.104}$$

where

$$M = \begin{pmatrix} 1 + \frac{d\Psi_\chi}{d\chi} & -\frac{1}{\kappa - \varepsilon\kappa_a} \\ \frac{d\Psi_a}{d\chi} - \frac{d\Psi_\chi}{d\chi} & 1 + \frac{1}{\kappa - \varepsilon\kappa_a} \end{pmatrix} \tag{A.105}$$

We note that $I_{HB}/I_{max} = p_o = (1 + exp[\chi])^{-1}$ is in one-to-one corre-

spondence with the variable χ. Thus,

$$\chi = ln\left(\frac{p_o}{1-p_o}\right) \tag{A.106}$$

$$v = \frac{1}{p_o(1-p_o)}\frac{dp_o}{dt} \tag{A.107}$$

For given parameter values, we can use the Pade approximation to the coordinate-transformation equations to infer the position and velocity of the gating extension χ from the position X and velocity $u = \frac{dX}{dt}$ of the bundle beyond the linear response range.

In sum, from the dynamics X and u, the dynamics of χ and v can be inferred; conversely, from the dynamics of χ and v the dynamics of the X and u can be inferred. Since $X_a = X - \chi$, the dynhamics of any two of the variables χ, v, X, and u suffice to determine the dynamics of X and $\frac{dX_a}{dt}$

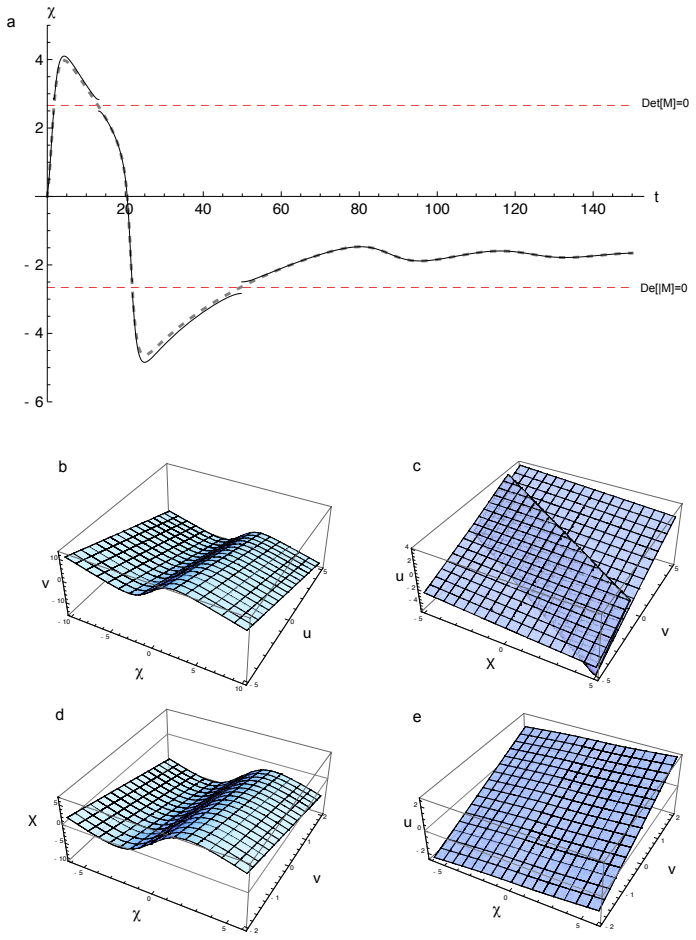

Figure A.1: *Coordinate transformations in the excitable regime* a. Dynamics of the χ inferred from the dynamics of X and $u = \frac{dX}{dt}$ In solid black, the solution derived analytically from the Pade-approximated model, given the trajectories of X and u. The horizontal lines show the values of χ at which the coordinate transformation is not locally invertible (i.e.: $Det(M) = 0$); at these lines, the Pade-approximated solution for χ jumps from one cubic branch to another. b. χ of X and $u = \frac{dX}{dt}$ c. v as a function of X and u. d) X as a function of χ and v. e) u as a function of χ and $\frac{d\chi}{dt}$ in the excitable underdamped parameter regime

A.3 Accuracy of the Pade approximation

Figure (A.2) shows that the error introduced by the Pade approximation remains small within the physiological range of the state variables, though a systematic discrepancy in the derivatives of the nullcline functions arises as $|\chi| \to \infty$. Nevertheless, within the physiological range, the Pade-approximated model affords an excellent approximation of the simplified model.

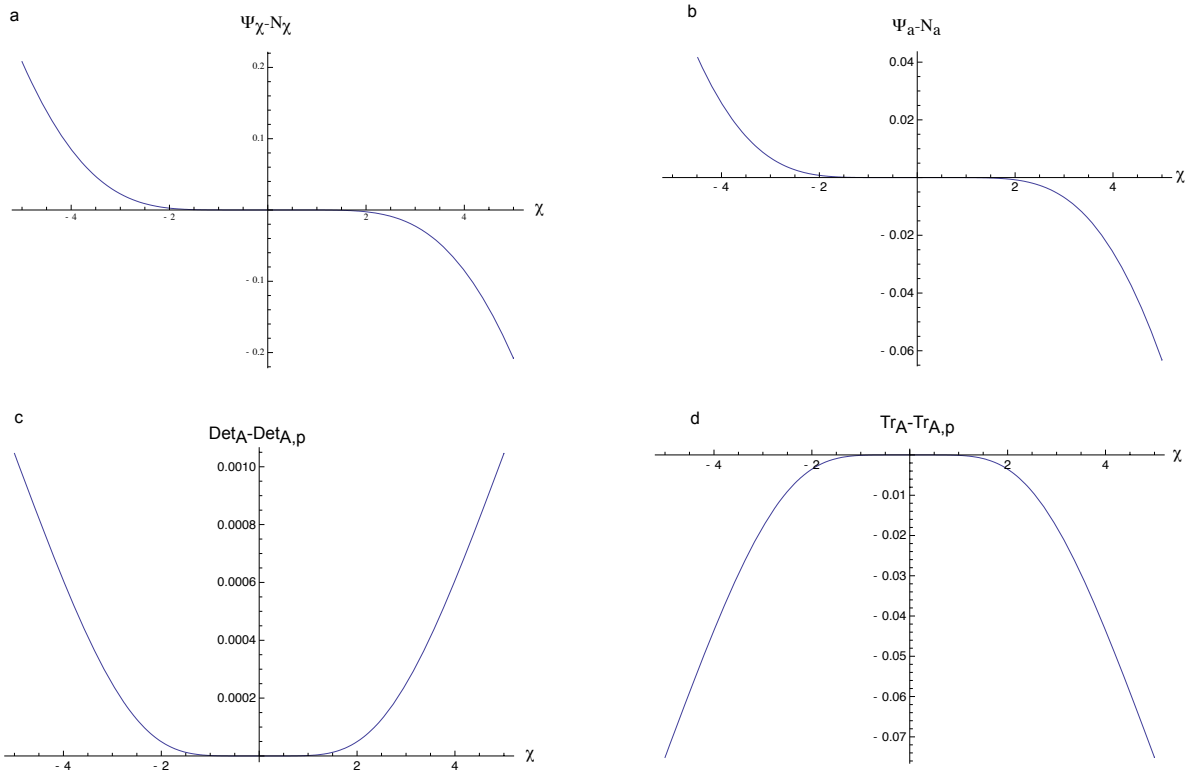

Figure A.2: *Accuracy of the Pade approximation*
Error associated with the order- (3,2) Pade approximation about zero of various functions of χ: a) Φ_χ; b) Φ_a; c) Det_A; and d) Tr_A. The parameter values for the error calculations illustrated here are: ($\varepsilon = 0.05$, $\eta = 8$, $\eta_a = 2$, $\kappa = 0.5$, $\kappa_a = 0.4$, $C_{Static} = -4.68$)

Appendix B

Bifurcation Structure

B.1 Normal-form approximation to the near-bifurcation dynamics

In this section, we undertake a perturbation analysis of the weakly nonlinear oscillations of the simplified model, using the method of normal forms.

Let Λ denote the matrix of eigenvalues of the simplified model, and let r_1 , r_2 denote the associated eigen-variables. We introduce the complex variable w

$$w =_{df} \nu\,(r_1 + ir_2) \tag{B.1}$$

where ν is some function of μ that tends to 0 as μ tends to 0. We then construct a *near-identity transformation* of the variables w_i to the variables u_i:

$$w_i = u_i + \sum_{j=1}^{N} \sum_{k=1}^{N} \nu^j \mu^k T_{jk} \left(u_{1,}, \ldots, u_n \right) \tag{B.2}$$

Consider a perturbation expansion in ν and μ of the dynamical equation for the variables:

$$\frac{du_i}{dt} = U_{00}^i + \nu U_{10}^i + \mu U_{01}^i + \nu^2 U_{20}^i + \mu\nu U_{01}^i + \mu^2 U_{02}^i \tag{B.3}$$

We assume that the T_{ij} have the form:

$$T_{jk} =_{df} \sum_{l=0}^{2} a_{jkl} u_1^l u_2^{2-l} \tag{B.4}$$

Finally, we set the coefficients a_{jkl} of the transformation such that, wherever possible, the non-linear terms are assigned a coefficient of zero in the

dynamical equation.

Figure B.1 shows predictions of the normal form approximations near a saddle-node bifurcation; and a supercritical Hopf bifurcation.

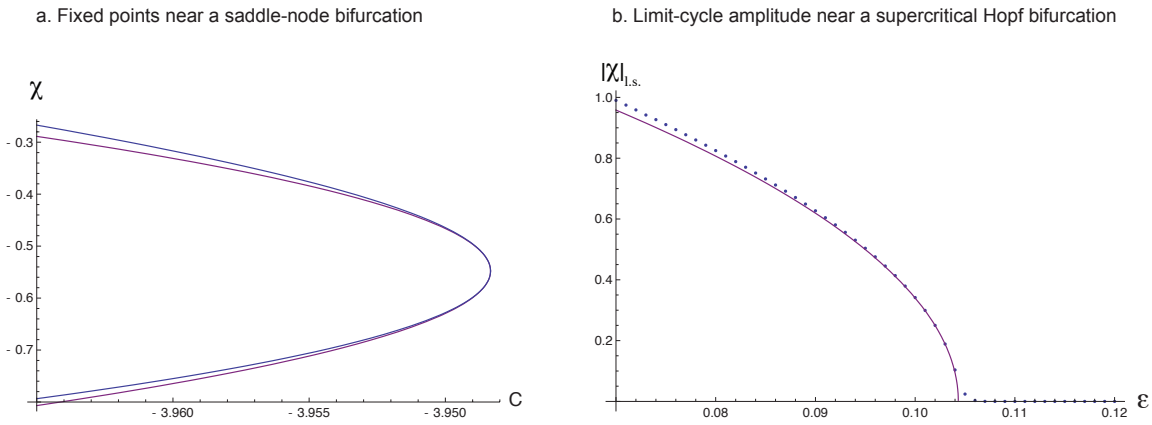

Figure B.1: *Predictions of saddle-node and Hopf normal-form approximations*

a.) Fixed points as a function of the parameter C, predicted by the saddle-node normal-form equation (purple) and the Pade approximation (blue). The remaining parameters have the values $\varepsilon = 0.05$, $\eta = 8$, $\eta_a = 0$, $\kappa = 0.6$, and $\kappa_a = 0.7$ b.) Limit-cycle amplitude as a function of the parameter ε, as predicted by the normal-form equation (purple), and calculated numerically (blue points). the remaining parameters have the values: ($\eta = 4.84374$, $\eta_a = 0.087394$, $\kappa = 0.5$, $\kappa_a = 1$ $C = -2.4$)

B.1.1 Saddle-node normal form

The topological normal form for the dynamics in the vicinity of a saddle-node bifurcation can readily be calculated for the various bifurcation parameters; For instance, for the static force parameter C the normal form is:

$$\frac{d\chi}{dt} = \varepsilon\kappa_a\,(C - C_{crit}) + \frac{1}{2}\omega^2 d_\kappa \frac{\partial^2 p_o}{\partial \chi^2}(\chi - \chi_{crit})^2 \tag{B.5}$$

B.1.2 Hopf normal form

Under the condition that the operating point is $\chi = 0$, the topological normal form at a Hopf bifurcation gives identical results to the multiple-scales solution below,

$$\frac{dz}{dt} = (\frac{\mu_0}{2} + i\sqrt{k_0})z - \frac{\mu_{nl}}{8}|z|^2 z \tag{B.6}$$

where

$$z = re^{i\theta} \tag{B.7}$$

$$\chi = r\cos(\theta) \quad , \quad X_a = -\left(\frac{1+\varepsilon-\frac{\alpha_\varepsilon}{4}}{\kappa - \varepsilon\kappa_a}\right) r\cos(\theta) - \sqrt{\varepsilon(\kappa + \kappa_a - \frac{\kappa_a\eta}{4})}\sin(\theta) \tag{B.8}$$

$$\mu_0 = -Tr_A(0) = 1+\varepsilon+\varepsilon\kappa_a-\frac{\alpha_\varepsilon}{4} \quad , \quad \mu_{nl} = \frac{\alpha_\varepsilon}{16} \quad , \quad k_0 = Det_A(0) = \omega^2(1-\frac{d_\kappa}{4}) \tag{B.9}$$

Bibliography

[1] Orszag S.A. Bender, C.M. *Advanced Methods for Scientists and Engineers*. Springer, New York, NY, 1999.

[2] Hudspeth A. J. Bozovic, D. Hair-bundle movements elicited by transepithelial electrical stimulation of hair cells in the sacculus of the bullfrog. *Proc Natl Acad Sci U S A*, 100(3):958–63, 2003.

[3] Duke T. Julicher F. Prost J. Camalet, S. Auditory sensitivity provided by self-tuned critical oscillations of hair cells. *Proc Natl Acad Sci U S A*, 97(7):3183–8, 2000.

[4] M Eugenia Chiappe, Andrei S Kozlov, and A J Hudspeth. The structural and functional differentiation of hair cells in a lizard's basilar papilla suggests an operational principle of amniote cochleas. *J Neurosci*, 27(44):11978–11985, 2007.

[5] D. P. Corey and A. J. Hudspeth. Kinetics of the receptor current in bullfrog saccular hair cells. *J Neurosci*, 3(5):962–76, 1983.

[6] W Denk and W W Webb. Forward and reverse transduction at the limit of sensitivity studied by correlating electrical and mechanical fluctuations in frog saccular hair cells. *Hear Res*, 60(1):89–102, 1992.

[7] V. M. Eguiluz, M. Ospeck, Y. Choe, A. J. Hudspeth, and M. O. Magnasco. Essential nonlinearities in hearing. *Phys Rev Lett*, 84(22):5232–5, 2000.

[8] J. Howard and A. J. Hudspeth. Mechanical relaxation of the hair bundle mediates adaptation in mechanoelectrical transduction by the bullfrog's saccular hair cell. *Proc Natl Acad Sci U S A*, 84(9):3064–8, 1987.

[9] A J Hudspeth and R S Lewis. Kinetic analysis of voltage- and ion-dependent conductances in saccular hair cells of the bull-frog, rana catesbeiana. *J Physiol*, 400:237–274, 1988.

[10] A J Hudspeth and R S Lewis. A model for electrical resonance and frequency tuning in saccular hair cells of the bull-frog, rana catesbeiana. *J Physiol*, 400:275–297, 1988.

[11] Andrei S Kozlov, Thomas Risler, and A J Hudspeth. Coherent motion of stereocilia assures the concerted gating of hair-cell transduction channels. *Nat Neurosci*, 10(1):87–92, 2007.

[12] R S Lewis and A J Hudspeth. Voltage- and ion-dependent conductances in solitary vertebrate hair cells. *Nature*, 304(5926):538–541, 1983.

[13] D Manoussaki, E K Dimitriadis, and R S Chadwick. Cochlea's graded curvature effect on low frequency waves. *Phys Rev Lett*, 96(8):088701, 2006.

[14] P. Martin, D. Bozovic, Y. Choe, and A. J. Hudspeth. Spontaneous oscillation by hair bundles of the bullfrog's sacculus. *J Neurosci*, 23(11):4533–48, 2003.

[15] P. M. Narins and E. R. Lewis. The vertebrate ear as an exquisite seismic sensor. *J Acoust Soc Am*, 76(5):1384–7, 1984.

[16] SK Schultz. Principles of neural science, 4th edition., 2001. American Journal of Psychiatry.

[17] G. M. Shepherd and D. P. Corey. The extent of adaptation in bullfrog saccular hair cells. *J Neurosci*, 14(10):6217–29, 1994.

[18] Fenton MB. O'Farrell MJ. Simmons, JA. Echoloation and pursuit of prey by bats. *Science*, 203:16–21, Jan 1979.

[19] T. M. Squires. Optimizing the vertebrate vestibular semicircular canal: could we balance any better? *Phys Rev Lett*, 93(19):198106, 2004. 0031-9007 (Print) Journal Article.

[20] J Triblehorn and D Yager. Timing of praying mantis evasive responses during simulated bat attack sequences. *Journal of Experimental Biology*, Jan 2005.

[21] Georg Von Békésy. *Experiments in hearing.* McGraw-Hill, New York, 1960.

[22] Suga N. Xiao, Z. Modulation of cochlear hair cells by the auditory cortex in the mustached bat. *Nature neuroscience*, 5(1):57–63, 2002.